Molecular Therapy
Methods & Clinical Development
Original Article

VEGFD Protects Retinal Ganglion Cells and, consequently, Capillaries against Excitotoxic Injury

Annabelle Schlüter,[1] Bahar Aksan,[1] Ricarda Diem,[2,3] Richard Fairless,[2,3] and Daniela Mauceri[1]

[1]Department of Neurobiology, Interdisciplinary Center for Neurosciences, Heidelberg University, Im Neuenheimer Feld 366, 69120 Heidelberg, Germany; [2]Department of Neurology, University Clinic Heidelberg, Im Neuenheimer Feld 368, 69120 Heidelberg, Germany; [3]CCU Neurooncology, German Cancer Consortium (DKTK), German Cancer Research Centre (DKFZ), 69120 Heidelberg, Germany

In the central nervous system, neurons and the vasculature influence each other. While it is well described that a functional vascular system is trophic to neurons and that vascular damage contributes to neurodegeneration, the opposite scenario in which neural damage might impact the microvasculature is less defined. In this study, using an *in vivo* excitotoxic approach in adult mice as a tool to cause specific damage to retinal ganglion cells, we detected subsequent damage to endothelial cells in retinal capillaries. Furthermore, we detected decreased expression of vascular endothelial growth factor D (VEGFD) in retinal ganglion cells. *In vivo* VEGFD supplementation via neuronal-specific viral-mediated expression or acute intravitreal delivery of the mature protein preserved the structural and functional integrity of retinal ganglion cells against excitotoxicity and, additionally, spared endothelial cells from degeneration. Viral-mediated suppression of expression of the VEGFD-binding receptor VEGFR3 in retinal ganglion cells revealed that VEGFD exerts its protective capacity directly on retinal ganglion cells, while protection of endothelial cells is the result of upheld neuronal integrity. These findings suggest that VEGFD supplementation might be a novel, clinically applicable approach for neuronal and vascular protection.

INTRODUCTION

In the central nervous system (CNS), the neuronal and vascular components have a strong structural and functional interdependence during both development and adulthood.[1] In the retina, in particular, a tight coupling between retinal ganglion cells (RGCs) and capillaries has been described,[2] but the molecular and cellular players underlying this link have not been completely elucidated. Members of the vascular endothelial growth factor (VEGF) family have been reported to be possible modulators of the communication between the vascular and neuronal compartments.[3–6]

The retinal neurovascular interface plays a role not only in physiology but also in several pathologies. Dysfunctions of both the neural and vascular components have been implicated in pathologies of the visual system such as glaucoma, diabetic retinopathy, and macular degeneration.[2] It is well known that vascular occlusion and damage can contribute to the progression of neural retina injury[7] while the putative impact of neuronal damage onto the integrity of the capillaries is unclear. In experimental models of neural retinal injury, delayed damage to the retinal microvasculature has been observed,[8–10] suggesting that neural integrity may indeed be critical for vascular health.

Capillaries have a small diameter and consist of a single endothelial cell (EC) layer forming the inner lining, which is anchored to the basement membrane (BM). A well-reported phenomenon, which has no clear explanation for its occurrence, is the detected higher number of empty sleeves throughout the CNS (retina, hippocampus, and cortex) in relationship to both physiological aging and to several neurodegenerative diseases.[11–13] Empty sleeves, also named string vessels or acellular capillaries, consist of remnants of BM, which have lost the inner ECs and, in several cases, have collapsed.[11] Empty sleeves cannot transport blood or plasma, as they are not perfused[11] and thus may have noxious effects on the surrounding tissue and enhance degeneration. It is not known what drives the formation of empty sleeves; however, their increased presence following neuronal degeneration indicates that neurons might play a role.

In this study, we used an *in vivo* approach to cause specific damage to RGCs, which we found to be accompanied by a reduction in the expression of VEGFD, a member of the VEGF family, in RGCs and by the formation of empty sleeves. We additionally reveal the protective capacity of VEGFD against degeneration of RGCs and, as a result of the maintained neuronal integrity, also against capillary damage. Our data indicate that VEGFD delivery might provide a promising therapeutic strategy for the treatment of degenerative diseases of the neuronal and vascular system.

Received 25 September 2019; accepted 19 December 2019;
https://doi.org/10.1016/j.omtm.2019.12.009.

Correspondence: Daniela Mauceri, PhD, Department of Neurobiology, Interdisciplinary Center for Neurosciences, Heidelberg University, Im Neuenheimer Feld 366, 69120 Heidelberg, Germany.
E-mail: mauceri@nbio.uni-heidelberg.de

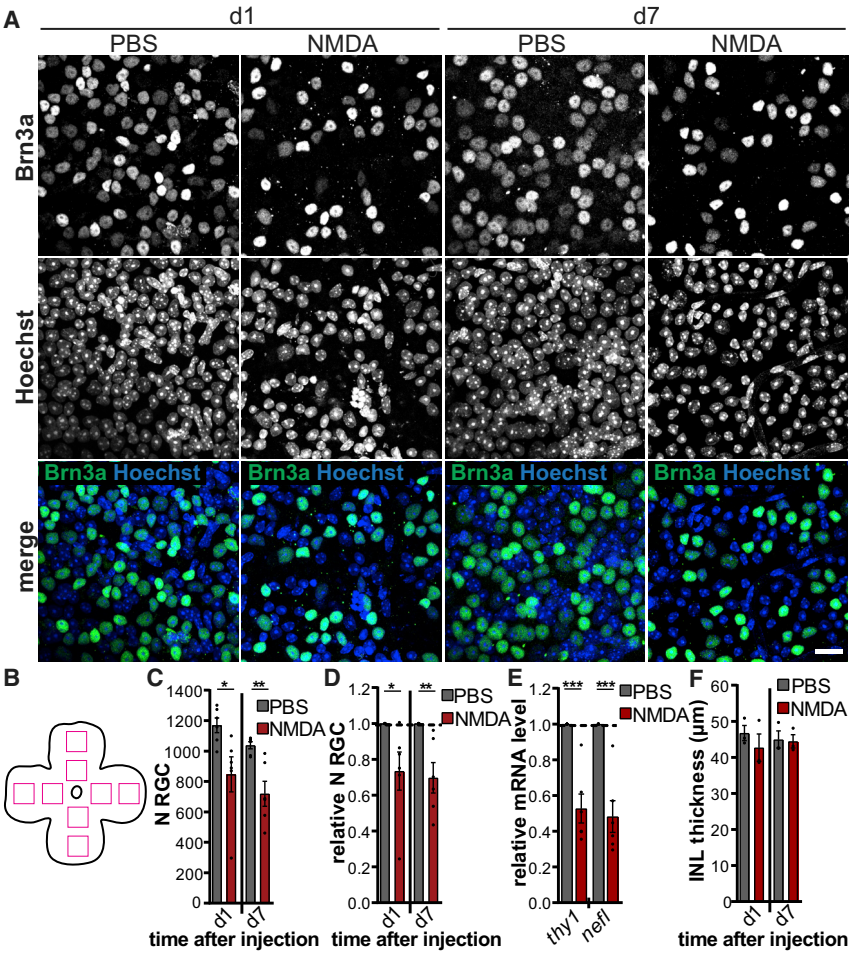

Figure 1. NMDA-Triggered Excitotoxicity Induces RGC Death

(A) Representative images of retinal whole mounts at d1 and d7 after intravitreal injections of NMDA or PBS. RGCs were immunolabeled using an antibody against Brn3a (green); nuclei were labeled with Hoechst (blue). Scale bar, 20 µm. (B) Schematic of the fields used for quantification in retinal whole mounts in central and peripheral parts of the retina. (C) Quantification of RGCs in retinas injected as indicated. Unpaired t test. n = 6. PBS versus NMDA (d1), p = 0.0274; PBS versus NMDA (d7), p = 0.0038. (D) Quantification of RGCs in retinas injected as indicated. RGC numbers in the NMDA-treated eye were normalized to the PBS control eye from the same animal. Unpaired t test. n = 6. PBS versus NMDA (d1), p = 0.0318; PBS versus NMDA (d7), p = 0.0051. (E) qRT-PCR analysis of *thy1* and *nefl* expression in retinas 1 day after intravitreal injection of NMDA. Unpaired t test. n = 6. *thy1*, p = 0.0002; *nefl*, p = 0.0002. (F) Quantification of INL thickness in sagittal retina sections injected as indicated. Unpaired t test. n = 3. PBS versus NMDA (d1), p = 0.4015; PBS versus NMDA (d7), p = 0.8741. Bars represent mean ± SEM. Dots represent single values. *p < 0.05, **p < 0.01, ***p < 0.001.

RESULTS

Excitotoxicity is a pathological phenomenon leading to neuronal damage or death that has been associated with several disorders of the nervous system.[14] *N*-methyl-D-aspartate (NMDA) receptors (NMDARs), calcium-permeable channels, are the principal initiators of excitotoxic cell death induced by excessive receptor activation either by high glutamate levels or NMDA exposure.[14,15] In the eye, excitotoxicity has been linked to glaucoma, retinal ischemia, and diabetic retinopathy.[16–20] Indeed, high concentrations of glutamate or NMDA delivered via intravitreal injections can be utilized as a tool to cause RGC death *in vivo*.[21–26] We performed a single intravitreal injection of 10 nmol of NMDA in adult mice and analyzed NMDA-induced RGC death at two different time points (day 1 [d1] and day 7 [d7]) (Figure 1). Brn3a served as a marker to identify and quantify RGCs[27] in central and peripheral regions of retinal whole mounts (Figures 1A and 1B). One day after intravitreal NMDA injections, the number of RGCs was significantly decreased compared to the PBS-injected control eyes (Figures 1A–1D). RGC death did not worsen over time, as observed by comparable RGC survival 7 days after the NMDAR-mediated excitotoxic insult (Figures 1C and 1D). We further detected a significant reduction in the mRNA levels of the RGC markers *thy1* and *nefl* (Figure 1E) in retinal homogenates. To investigate whether intravitreal injection of NMDA damages other retinal neurons than RGCs, we measured the thickness of the inner nuclear layer (INL) as an indication of possible cell death in the INL.[28] We did not detect any significant changes after intravitreal NMDA injections (Figure 1F). A terminal deoxynucleotidyltransferase-mediated dUTP nick end labeling (TUNEL) assay carried out on retinal sections confirmed that the extent of apoptosis in retinal tissue following an intravitreal injection of 10 nmol of NMDA was negligible in the INL (percentage of TUNEL$^+$ cells: d1, PBS (0.02949081%) versus NMDA (0.6696871%), p = 0.2019; d7, PBS (0.09155836%) versus NMDA (0.08281018%), p = 0.7552; unpaired Student's t test, n = 3) and outer nuclear layer (ONL; percentage of TUNEL$^+$ cells: d1, PBS (0.07544173%) versus NMDA (0.05547914%), p = 0.7181; d7, PBS (0.05516085%) versus NMDA (0.0662406%), p = 0.6445; unpaired Student's t test, n = 3). Taken together, these data demonstrate that intravitreal injection of NMDA can be used to trigger degeneration of RGCs in the retina *in vivo*.

In the retina, RGCs are structurally and functionally coupled with capillaries, and dysfunctions of both the neural and vascular components are present in pathologies of the visual system.[2] We proceeded to analyze the possible effects of the *in vivo* NMDA insult on the retinal capillaries. We found that intravitreal injection of NMDA promoted the formation of collapsed empty sleeves at both d1 and d7 assessed by immunostaining of the BM with anti-collagen IV and labeling of the ECs with isolectin B4 (Figures 2A–2C). Using electron microscopy, it was possible to observe, in some cases, occluded lumen of the capillaries due to swelling of the

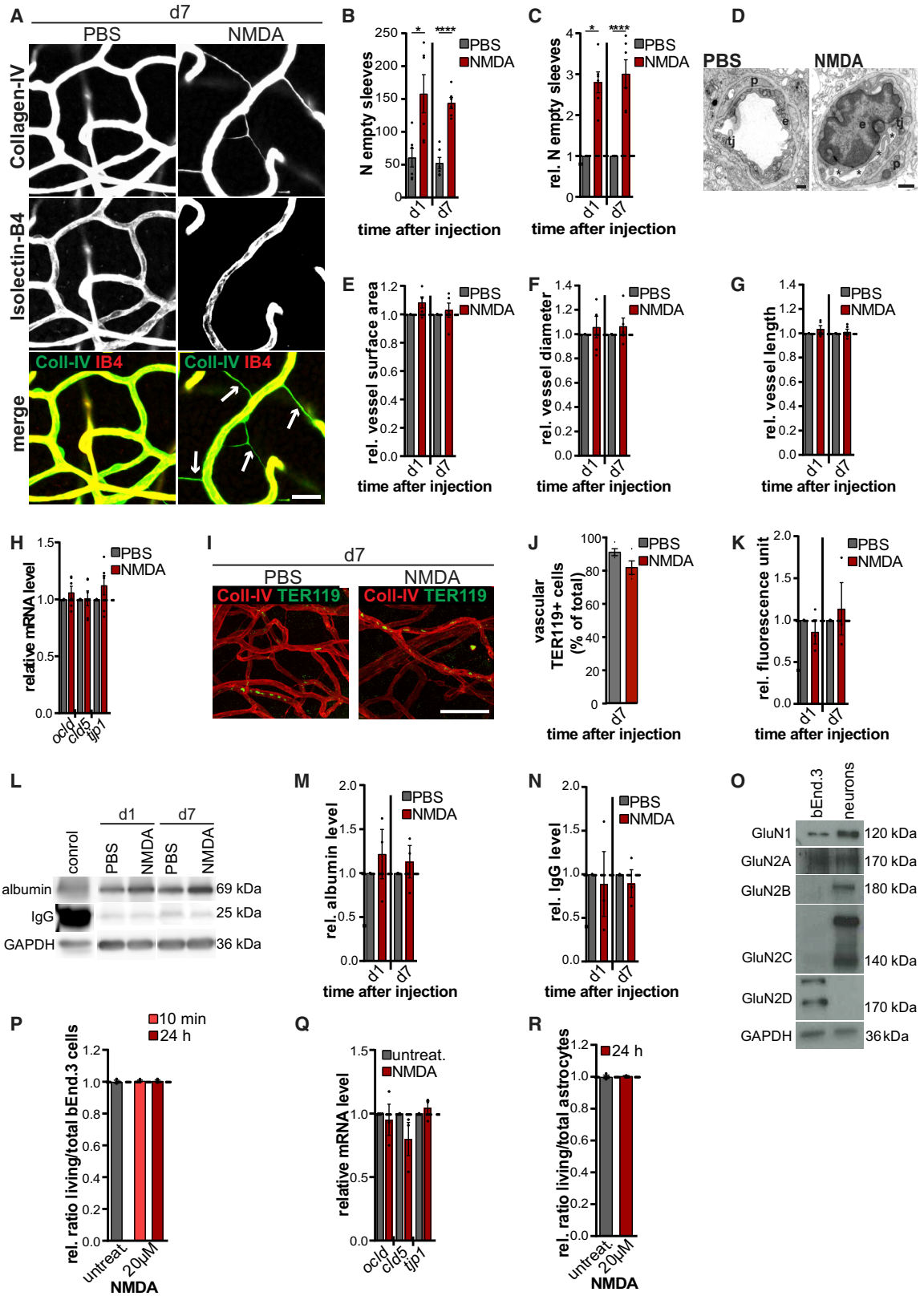

(legend on next page)

damaged ECs prior to their death and removal,[29,30] whereas tight junctions remained intact (Figure 2D). The increased presence of collapsed empty sleeves appeared to be a specific phenomenon, as other vascular parameters, such as vessel surface area, vessel diameter, and vessel length, were not affected by the NMDA insult at any of the analyzed time points (Figures 2E–2G). To assess potential NMDA-mediated effects on the blood-retinal barrier (BRB), we first analyzed in retinal homogenates the mRNA levels of *ocld*, *cld5*, or *tjp1*, encoding for occludin, claudin-5, and ZO-1 respectively, molecules important for the functionality of endothelial tight junctions. None of the analyzed genes was affected by intravitreal NMDA injection (Figure 2H). To clarify whether intravitreal NMDA injection could prompt extravasation of cells, we assessed the percentage of erythrocytes within the retina capillaries[31] in relationship to the total amount of erythrocytes within and outside vessels. We found no difference between PBS-injected controls and NMDA-injected retinas (Figures 2I and 2J). Furthermore, in whole-retina extracts, we examined the extravasation of intravenously injected 3-kDa dextran-fluorescein as well as of endogenous albumin and immunoglobulin G (IgG) following intravitreal NMDA injections,[30] which we found similar to PBS-injected controls (Figures 2K–2N). These data indicate that NMDA-triggered excitotoxicity, in addition to promoting death of RGCs, causes increased formation of empty sleeves without affecting BRB functionality or the overall structure of the vascular network.

ECs of the CNS express NMDA receptors[32–36] and might therefore be a direct target of NMDAR-mediated toxicity. To understand whether the observed degeneration of ECs following NMDA intravitreal injection is the result of a direct or indirect effect of NMDA, we used a different approach and directly exposed only ECs to NMDA *in vitro*. We confirmed the expression of the GluN1 channel-forming subunit of the NMDA receptor as well as of the regulatory subunits GluN2A and GluN2D (Figure 2O) in a mouse brain EC line (bEnd.3).[34,37] GluN2B and GluN2C subunits were not detected. We decided to compare the sensitivity of cultured neurons and ECs to NMDA using exposure to 20 μM NMDA, which typically causes fast neuronal death.[38] When treated with 20 μM NMDA acutely for 10 min or for 24 h, the vitality of the cultured mouse brain ECs remained unaltered (Figure 2P) while neurons considerably died.[38] Even using a higher NMDA concentration (1 mM), close to the one reached *in vivo* after intravitreal injection of 10 nmol of NMDA in the relatively small volume of the mouse eye, while neuronal death rate reached 100%, the vitality of cultured ECs was still unaffected (untreated versus NMDA 10 min, n = 3, p = 0.9868; untreated versus NMDA 24 h, n = 3, p = 0.6556; unpaired Student's t test.) The expression levels of *ocld*, *cld5*, and *tjp1* of NMDA-treated cultured ECs were also similar to those of control-treated cells (Figure 2Q). In the mammalian neurovascular unit, astrocytes represent a considerable percentage of the present cells and can exchange signals with ECs.[39] Moreover, numerous studies revealed the functional expression of NMDARs on various types of glia cells in the nervous system.[40] In

Figure 2. Intravitreal Injection of NMDA Induces Formation of Empty Sleeves via an Indirect Mechanism

(A) Representative images of retinal whole mounts at d7 after intravitreal injections of NMDA or PBS. Vessels were immunolabeled with antibodies against collagen IV (green) and isolectin B4 (red). Arrows indicate empty sleeves. Scale bar, 20 μm. (B) Quantification of empty sleeves in retinas injected as indicated. Unpaired t test. n = 6. PBS versus NMDA (d1), p = 0.0129; PBS versus NMDA (d7), p < 0.0001. (C) Quantification of empty sleeves in retinas injected as indicated. Number of empty sleeves in the NMDA-treated eye were normalized to the PBS control eye from the same animal. Unpaired t test. n = 6. PBS versus NMDA (d1), p < 0.0001; PBS versus NMDA (d7), p = 0.0002. (D) Representative images of electron microscopy of retinas injected as indicated. Left: Normal capillary in retinas of PBS-injected eyes with ECs (e), tight junctions (tj), and pericyte (p). Scale bar, 5,000 nm. Right: Capillary with swollen EC (e) in retinas of NMDA-injected eyes. Asterisks indicate occluded lumen. Tight junctions (tj) and pericytes (p) were still intact. Scale bar, 500 nm. (E) Quantification of vessel surface area in retinas injected as indicated. Surface area in the NMDA-treated eye was normalized to the PBS control eye from the same animal. Unpaired t test. n = 6. PBS versus NMDA (d1), p = 0.0626; PBS versus NMDA (d7), p = 0.5847. (F) Quantification of vessel diameter in retinas injected as indicated. Diameter in the NMDA-treated eye was normalized to the PBS control eye from the same animal. Unpaired t test. n = 6. PBS versus NMDA (d1), p = 0.5313; PBS versus NMDA (d7), p = 0.3695. (G) Quantification of vessel fiber length in retinas injected as indicated. Fiber length in the NMDA-treated eye was normalized to the PBS control eye from the same animal. Unpaired t test. n = 6. PBS versus NMDA (d1), p = 0.2375; PBS versus NMDA (d7), p = 0.6235. (H) qRT-PCR analysis of *ocld*, *cld5*, and *tjp1* expression in retinas of mice 7 days after intravitreal injection of PBS and NMDA. Unpaired t test. n = 6. *ocld*, p = 0.2803; *cld5*, p = 0.8959; *tjp1*, p = 0.1733. (I) Representative images of retinal whole mounts at d7 after intravitreal injections of NMDA or PBS. Vessels were immunolabeled with antibodies against collagen IV (red) and erythrocytes with antibodies against TER119 (green). Scale bar, 50 μm. (J) Quantification of vascular erythrocytes in retinas injected as indicated and expressed as percentage of the total number of erythrocytes present in the analyzed images (within and outside vessels). Unpaired t test. n = 4. PBS versus NMDA (d7), p = 0.088. (K) Quantification of dextran-fluorescein (3 kDa) extravasation in retinal extracts 1 and 7 days after intravitreal PBS and NMDA injections. Unpaired t test. n = 3. PBS versus NMDA (d1), p = 0.3799; PBS versus NMDA (d7), p = 0.6891. (L) Representative immunoblots of albumin, IgG, and GAPDH in retinas of unperfused mice (control) or in retinas of perfused mice 1 and 7 days after intravitreal PBS and NMDA injections. (M) Quantification of albumin levels in retinal lysates injected as indicated. GAPDH was used for control of the amount of protein. Samples from the NMDA-treated eye were normalized to the PBS control eye from the same animal. Unpaired t test. n = 3. PBS versus NMDA (d1), p = 0.4845; PBS versus NMDA (d7), p = 0.5231. (N) Quantification of IgG levels in retinal lysates injected as indicated. GAPDH was used for control of the amount of protein. Samples from the NMDA-treated eye were normalized to the PBS control eye from the same animal. Unpaired t test. n = 3. PBS versus NMDA (d1), p = 0.7794; PBS versus NMDA (d7), p = 0.5372. (O) Representative immunoblots of different NMDAR (GluN) subunits and GAPDH in brain ECs (bEnd.3, left lane) and primary hippocampal neurons (right lane). (P) Quantification of cultured brain ECs (bEnd.3) survival after 20 μM NMDA exposure *in vitro* for 10 min or 24 h. The number of living bEnd.3 cells was normalized to the number of total bEnd.3 cells as well as to the ratio of living/total cells in the control (untreated). One-way ANOVA, Bonferroni's *post hoc* test. n = 3. Untreated versus NMDA (10 min), p > 0.9999; untreated versus NMDA (24 h), p > 0.9999; NMDA (10 min) versus NMDA (24 h), p > 0.9999. (Q) qRT-PCR analysis of *ocld*, *cld5*, and *tjp1* expression in bEnd.3 cells with or without NMDA treatment. Unpaired t test. n = 6. *ocld*, p = 0.7118; *cld5*, p = 0.1998, *tjp1*, p = 0.4434. (R) Quantification of cultured primary astrocyte survival after 20 μM NMDA exposure for 24 h. The number of living astrocytes was normalized to the number of total astrocytes as well as to the ratio of living/total astrocytes in the control (untreated). Unpaired t test. n = 3. Untreated versus NMDA (24 h), p = 0.7016. Bars represent mean ± SEM. Dots represent single values. *p < 0.05, ****p < 0.0001.

a similar manner to that observed for cultured brain ECs, we found that application of NMDA for 24 h did not affect the survival of primary cultured astrocytes (Figure 2R). Collectively, these data indicate that the *in vivo* detected increased number of empty sleeves, due to loss of ECs, after NMDA-based insult (Figures 2A–2D) is likely mediated by an indirect mechanism.

By reducing the time of analysis following intravitreal injection of NMDA to 6 h, we found that loss of RGCs (40.2% ± 6.3%; NMDA versus PBS, n = 3, p = 0.0005) temporally precedes the formation of empty sleeves (105.9% ± 5.8% number of empty sleeves after NMDA treatment; NMDA versus PBS, n = 3, p = 0.5249). In experimental models of neural retinal damage, degeneration of the capillaries in correlation to RGC death has been observed,[7–10] but it is not yet understood if and how RGCs might impact the retinal microvasculature. We hypothesized that degeneration of RGCs could negatively impact capillaries via an alteration in the molecular crosstalk between RGCs and ECs. The vascular endothelial growth factor (VEGF) family members and their receptors (VEGFRs) play roles both in the vascular and nervous system where they regulate, for example, vascular development, angiogenesis, as well as axonal path finding, dendritic morphology, synaptic plasticity, neuroprotection, and cognition.[41–43] Recently, a novel function of neuronal VEGFR2 expression in the regulation of the crosstalk between neurons and ECs in the retina has been described,[6] and VEGFR3 has been detected outside the vasculature in neural elements of the retina.[44,45] We therefore evaluated the potential effects of NMDA intravitreal injection on the expression levels of VEGF family members and receptors. While no change was found for the mRNA levels of *vegf*, *vegfc*, *vegfr2* (*kdr*), or *vegfr3 (flt4)* in retinal homogenates, we detected a significant reduction in *vegfd* levels (Figure 3A). VEGFD, beyond its previously documented functions in angiogenesis and lymphangiogenesis,[42] is expressed also in neurons[46–48] and is fundamental for the maintenance of neuronal dendritic architecture and cognition.[43,49–51] We successfully detected *VEGFD* mRNA (Figure 3C) and VEGFD protein in RGCs in post-mortem human retinas (Figure 3B) as well as in adult mouse RGCs (Figure 3E). After intravitreal injection of NMDA, we found that VEGFD protein levels were specifically reduced in RGCs (Figures 3D and 3E). Recently, in agreement with our present findings, it was shown that bath application of NMDA to primary cultured neurons caused a rapid and progressive decline of *vegfd* mRNA levels (D.M., B. Buchthal, T.J. Hemstedt, U. Weiss, C.D. Klein, and H. Bading, unpublished data). Using a similar experimental strategy, namely NMDA treatment of cultured cells, we found that *vegfd* expression levels remained constant in both mouse cultured ECs (Figure 3F) and primary astrocytic cultures (Figure 3G) following 24 h of exposure to NMDA. Thus, an NMDA-mediated insult caused reduction of VEGFD expression in RGCs but not in other cell types.

We hypothesized that preventing VEGFD downregulation in RGCs might be beneficial for RGC survival after NMDA-triggered injury. We intravitreally injected adult wild-type mice with recombinant adeno-associated viruses (rAAVs) containing neuron-specific expression cassettes for VEGFD (rAAV-VEGFD)[43,50] or as control, LacZ (rAAV-LacZ), with additional hemagglutinin (HA; for rAAV-VEGFD) or Flag (for rAAV-LacZ) tags to facilitate their detection. Intravitreal injection of rAAVs is a robust method used successfully to achieve long-lasting, stable gene delivery[52] and is under consideration in clinical trials.[53] rAAV-VEGFD has been previously used effectively to boost neuronal expression of VEGFD[43,50] and does not infect cells of the microvasculature (Figure S1A). To investigate the protective capacities of neuronal overexpressed VEGFD against excitotoxic retinal damage, we subjected rAAV-LacZ- and rAAV-VEGFD-injected mice to NMDA-triggered excitotoxicity and quantified RGC degeneration at d7 after the excitotoxic insult. While NMDA injections caused robust RGC loss in rAAV-LacZ-injected mice, RGC survival after NMDA treatment in rAAV-VEGFD-injected mice was similar to PBS-injected control eyes (Figures 4A, 4C, and 4D). Furthermore, VEGFD overexpression in RGCs significantly protected RGC axons in the optic nerve from the NMDA-mediated excitotoxic damage assessed by measuring the increased presence of dephosphorylated neurofilaments (detected by SMI-32), as indication for axonal stress. After intravitreal NMDA injections, in rAAV-LacZ-injected mice, SMI-32-labeled clusters greatly increased in comparison to PBS-injected controls, while in rAAV-VEGFD-injected animals, their NMDA-triggered formation was blunted (Figures 4B, 4E, and 4F).

We proceeded to test whether providing VEGFD in an acute treatment, at the same time of the insult, would still spare RGCs from degeneration. We intravitreally co-injected recombinant mature VEGFD protein (rVEGFD) with either PBS or NMDA and determined RGC survival at d1 and d7 after injection (Figure 5). At both time points, rVEGFD prevented excitotoxic degeneration of RGCs (Figures 5A and 5C–5E). Furthermore, we found that acute delivery of rVEGFD was capable of reducing the formation of NMDA-triggered SMI-32^{+} clusters, indicative of axonal damage (Figures 5B, 5F, and 5G). As a control, we performed similar experiments by co-injecting a different recombinant protein, recombinant GFP (rGFP), instead of rVEGFD, with NMDA or PBS (Figures 5H–5L). rGFP treatment did not have any effects on RGC survival (Figures 5H–5J; Figure S2A) or axonal injury (Figures 5K and 5L; Figure S2B). In conclusion, these findings show the specific protective capacity of VEGFD on RGCs and axonal integrity in an NMDA-triggered excitotoxicity model.

We investigated whether VEGFD supplementation could also restore the functional properties of RGCs in addition to sparing them from structural degeneration and death (Figures 4 and 5). For this purpose, we measured the function of RGCs within the retina by performing pattern electroretinography in mice[54] subjected to NMDA-triggered excitotoxicity with or without co-injection of rVEGFD (Figure 6). NMDA-triggered excitotoxicity led to significantly decreased amplitudes at complex spatial frequencies (0.10 cycles per degree [cyc/deg]), which represent reduced neuronal activity in the retina. The supplementation of rVEGFD with NMDA was capable of restoring amplitudes to values comparable to those in PBS- or rVEGFD-injected control mice (Figures 6B and 6C). After sacrificing the mice, we confirmed, in agreement to

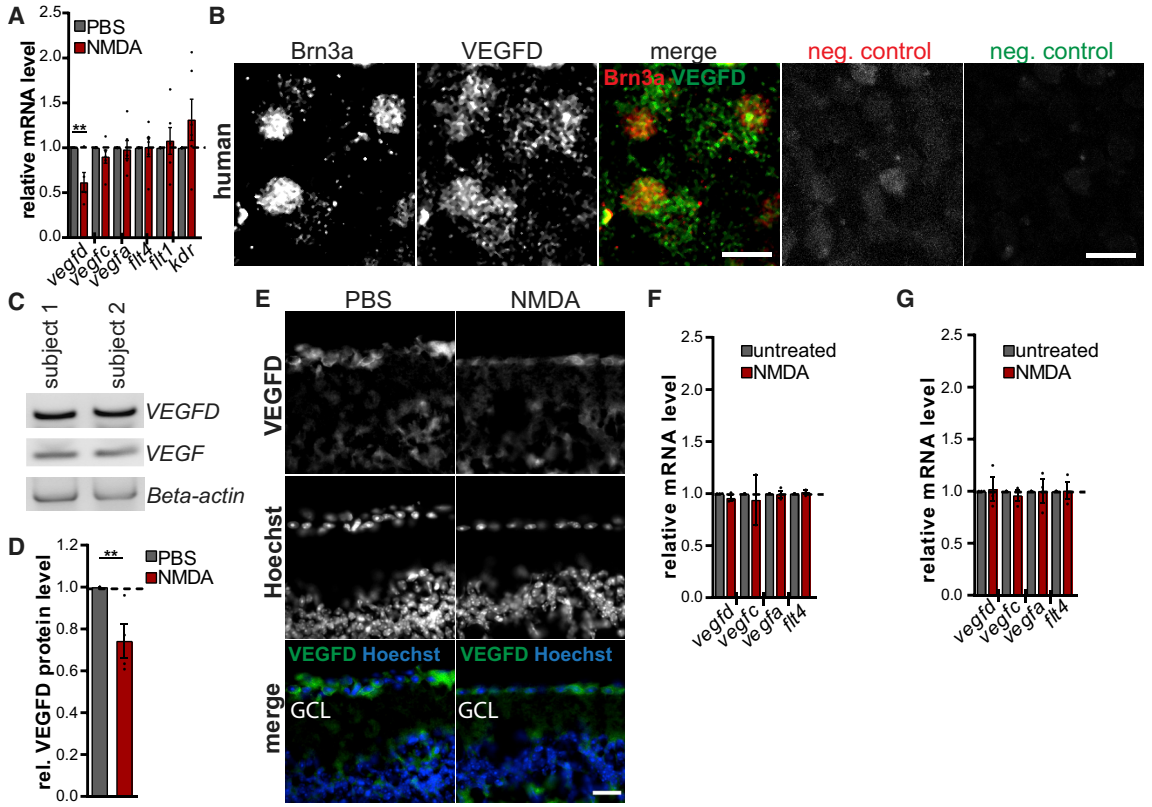

Figure 3. NMDA-Triggered Excitotoxicity Reduces VEGFD Expression in RGCs

(A) qRT-PCR analysis of *vegfd*, *vegfc*, *vegfa*, *flt4*, *flt1*, and *kdr* expression in retinal homogenates after intravitreal injection of NMDA. Unpaired t test. n = 6. *vegfd*, p = 0.0085; *vegfc*, p = 0.2052; *vegfa*, p = 0.8524; *flt4*, p = 0.9414; *flt1*, p = 0.6074; *kdr*, p = 0.2016. (B) Representative images of human retinal whole mounts. Retinas were immunolabeled with antibodies against Brn3a (red) and VEGFD (green). Scale bars, 10 μm. Negative controls of human retinas were immunolabeled only with secondary antibodies. (C) Representative bands of VEGFD, VEGFA, and β-actin cDNA products following qRT-PCR analysis of human retinal extracts obtained from two donors (subject 1, subject 2). (D) Quantification of VEGFD protein levels in cells in the ganglion cell layer of retinas of mice injected as indicated. Unpaired t test. n = 3. PBS versus NMDA, p = 0.0192. (E) Representative images of mouse sagittal retina sections at d7 after intravitreal injections of NMDA or PBS. Retinas were immunolabeled for VEGFD (green). Nuclei were labeled with Hoechst (blue). GCL, ganglion cell layer. Scale bar, 20 μm. (F) qRT-PCR analysis of *vegfd*, *vegfc*, *vegfa*, and *flt4* expression in brain ECs (b.END3) 24 h after 20 μM NMDA treatment. Unpaired t test. n = 3. *vegfd*, p = 0.1744; *vegfc*, p = 0.7598; *vegfa*, p = 0.8998; *flt4*, p = 0.4457. (G) qRT-PCR analysis of *vegfd*, *vegfc*, *vegfa*, and *flt4* expression in primary astrocytes 24 h after 20 μM NMDA treatment. Unpaired t test. n = 3. *vegfd*, p = 0.8716; *vegfc*, p = 0.4918; *vegfa*, p = 0.9902; *flt4*, p = 0.9331. Bars represent mean ± SEM. Dots represent single values. **p < 0.01.

what was assessed previously (Figure 5), that intravitreal NMDA injections resulted in significant RGC loss (48.52% ± 11.52%), which was reduced after rVEGFD supplementation (19.78% ± 4.55%). In summary, our data show the potential therapeutic capacity of intravitreal VEGFD supplementation in the maintenance of functional and intact RGCs.

Next, we tested whether supplementation of VEGFD could also spare the retinal microvasculature from NMDA-triggered excitotoxic damage (Figure 2). When VEGFD was specifically overexpressed in RGCs via rAAV-VEGFD (Figure S1), the formation of collapsed empty sleeves at d7 after the NMDA-triggered excitotoxic insult was reduced in comparison to control mice injected with rAAV-LacZ (Figures 7A, 7C, and 7D). Acute VEGFD treatment via co-injection of rVEGFD led to similar results displaying a significant decrease in the number of empty sleeves at d1 and d7 after NMDA treatment (Figures 7B and 7E–7G). Delivery of rGFP did not affect the NMDA-triggered formation of empty sleeves (Figures 7H–7J; Figure S2C), indicating a specific protective effect of VEGFD against NMDA-triggered vascular damage.

Our data show that an NMDA-mediated excitotoxic insult decreases the levels of VEGFD specifically in RGCs and triggers RGC degeneration prior to promoting formation of empty sleeves, likely via an indirect mechanism. Increasing VEGFD levels blunts the excitotoxicity-induced degeneration of both RGCs and ECs. In humans, VEGFD binds and activates both VEGFR2 and VEGFR3, whereas murine VEGFD exclusively activates VEGFR3.[55] To better elucidate whether capillaries are spared from excitotoxic damage as a consequence of VEGFD-mediated effects on neuronal survival or via a possible direct trophic simultaneous action of VEGFD on ECs, we used an approach to specifically reduce the expression of VEGFR3 in RGCs[45] while

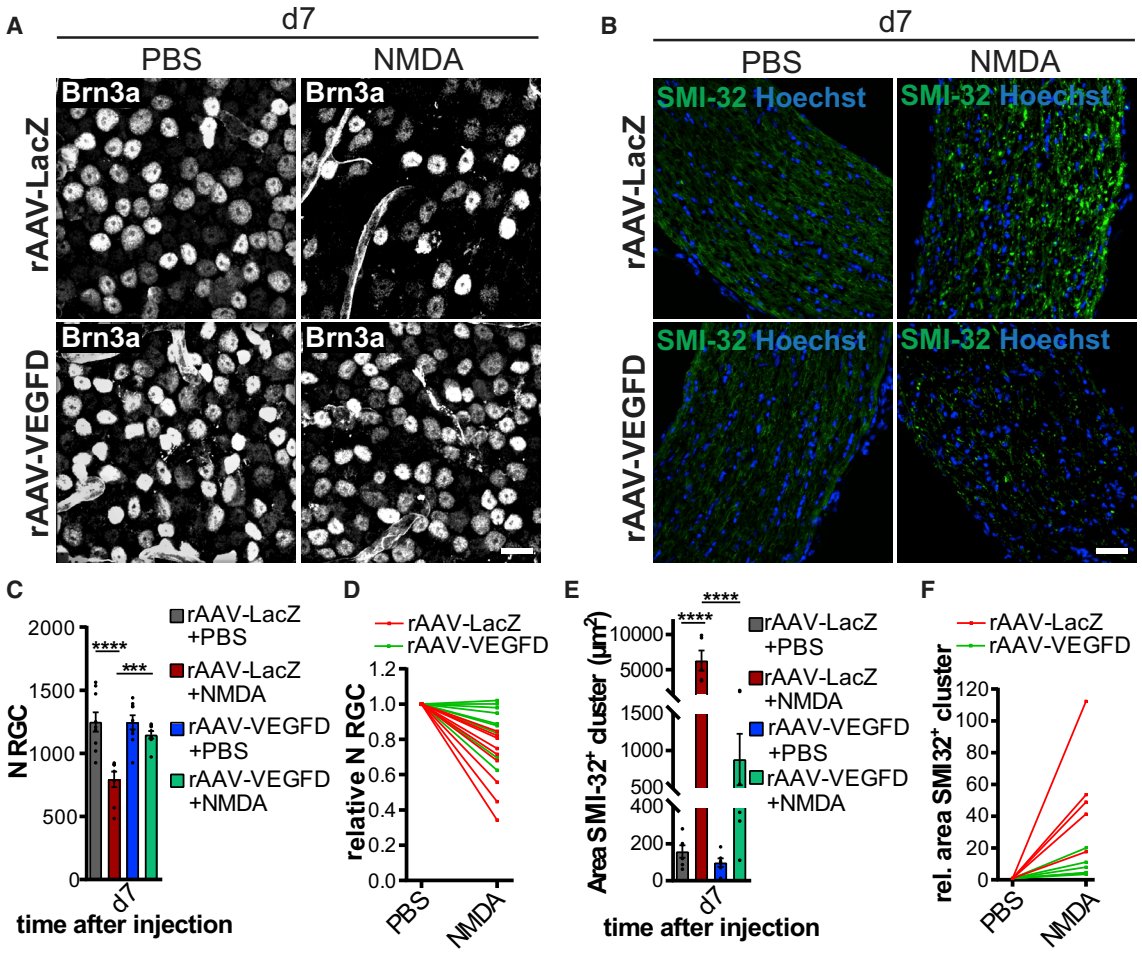

Figure 4. VEGFD Overexpression in RGCs Protects Them from NMDA-Mediated Damage

(A) Representative images of retinal whole mounts at d7 after intravitreal injections of NMDA or PBS from mice injected either with rAAV-LacZ or rAAV-VEGFD as indicated. RGCs were immunolabeled against Brn3a (green). Scale bar, 15 µm. (B) Representative images of sagittal optic nerve sections injected as indicated. Stressed axons were immunolabeled using SMI-32 (green). Nuclei were labeled using Hoechst (blue). Scale bar, 50 µm. (C) Quantification of RGCs injected as indicated. Two-way ANOVA, Bonferroni's *post hoc* test. n = 9. rAAV-LacZ+PBS versus rAAV-LacZ+NMDA, $p < 0.0001$; rAAV-VEGFD+PBS versus rAAV-VEGFD+NMDA, $p = 0.5035$; rAAV-LacZ+PBS versus rAAV-VEGFD+PBS, $p > 0.9999$; rAAV-LacZ+NMDA versus rAAV-VEGFD+NMDA, $p = 0.0006$. (D) Quantification of RGCs injected as indicated. RGC numbers in the NMDA-treated eye were normalized to the PBS control eye from the same animal. n = 9. (E) Quantification of SMI-32$^+$ clusters in optic nerves from eyes injected as indicated. Two-way ANOVA, Bonferroni's *post hoc* test. n = 6. rAAV-LacZ+PBS versus rAAV-LacZ+NMDA, $p < 0.0001$; rAAV-VEGFD+PBS versus rAAV-VEGFD+NMDA, $p = 0.7794$; rAAV-LacZ+PBS versus rAAV-VEGFD+PBS, $p > 0.9999$; rAAV-LacZ+NMDA versus rAAV-VEGFD+NMDA, $p < 0.0001$. (F) Quantification of SMI-32$^+$ clusters in optic nerves from eyes injected as indicated. SMI-32$^+$ clusters in the NMDA-treated eye were normalized to the PBS control eye from the same animal. n = 6. Bars represent mean ± SEM. Dots represent single values. ***$p < 0.001$, ****$p < 0.0001$. See also Figure S1.

leaving the expression unaltered in ECs. There are no satisfactory inducible cre-driver lines, which would guarantee efficient and extensive manipulation of the diverse RGC subtypes without affecting other retinal neurons and cell types.[56–58] Thus, we decided to employ intravitreal injection of rAAV-shVEGFR3[43] encoding short hairpin RNAs (shRNAs) targeting the mouse *Flt4* (*VEGFR3*) mRNA inserted downstream of the U6 promoter of the rAAV vector or, as control, a scrambled version rAAV-shSCR. The used rAAVs have been previously extensively characterized[43] and carry an mCherry expression cassette allowing for detection of infected neurons. Three weeks after intravitreal rAAV delivery, the infection rate of Brn3a$^+$ RGCs was above 60%. Other cell types within the retina, including cells of the vascular system, were not transduced by the used viruses (Figure S1C). Three weeks after infection, we performed intravitreal NMDA injections with or without co-injection of rVEGFD. Using this strategy, VEGFD cannot act on RGCs any longer—as they do not express VEGFR3–while they are still vulnerable to NMDA. In control mice that were intravitreally injected with rAAV-shSCR, NMDA caused significant RGC loss, which was prevented by intravitreal supplementation of rVEGFD (Figures 8A–8C), as expected. When VEGFR3 expression in RGCs was specifically reduced via rAAV-shVEGFR3, the VEGFD-mediated protection of RGCs from excitotoxicity was

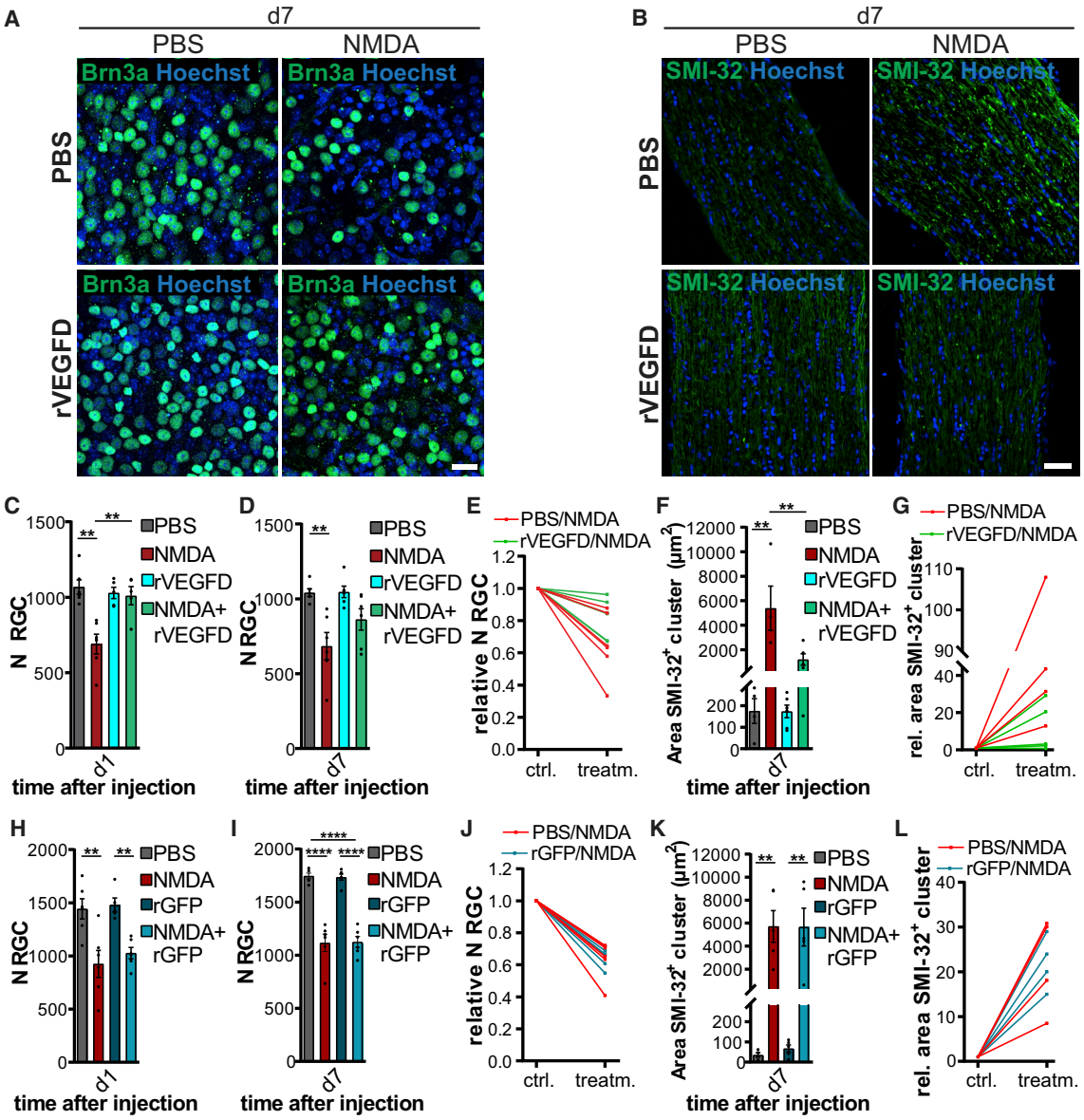

Figure 5. Recombinant VEGFD Protects RGCs from NMDA-Mediated Damage

(A) Representative images of retinal whole mounts at d7 after intravitreal injections of PBS, NMDA, rVEGFD, or rVEGFD+NMDA as indicated. RGCs were immunolabeled against Brn3a (green). Nuclei were immunolabeled with Hoechst (blue). Scale bar, 40 µm. (B) Representative images of sagittal optic nerve sections injected as indicated in (A). Stressed axons were immunolabeled using SMI-32 (green). Nuclei were labeled using Hoechst (blue). Scale bar, 50 µm. (C) Quantification of RGCs at d1 after intravitreal injections, injected as indicated in (A). Two-way ANOVA, Bonferroni's *post hoc* test. n = 6. PBS versus NMDA (sham), p = 0.0002; PBS versus NMDA (rVEGFD), p > 0.9999; sham versus rVEGFD (PBS), p > 0.9999; sham versus rVEGFD (NMDA), p = 00013. (D) Quantification of RGCs at d7 after intravitreal injections, injected as indicated in (A). Two-way ANOVA, Bonferroni's *post hoc* test. n = 6. PBS versus NMDA (sham), p = 0.0012; PBS versus NMDA (rVEGFD), p = 0.0973; sham versus rVEGFD (PBS), p > 0.9999; sham versus rVEGFD (NMDA), p = 0.1102. (E) Quantification of RGCs at d7 after intravitreal injections, injected as indicated in (A). RGC numbers in the NMDA-treated eye were normalized to the PBS control eye from the same animal. n = 6. (F) Quantification of SMI-32$^+$ clusters in optic nerves at d7 after intravitreal injections, injected as indicated in (A). Two-way ANOVA, Bonferroni's *post hoc* test. n = 6. PBS versus NMDA (sham), p = 0.0012; PBS versus NMDA (rVEGFD), p = 0.6742; sham versus rVEGFD (PBS), p > 0.9999; sham versus rVEGFD (NMDA), p = 0.0047. (G) Quantification of SMI-32$^+$ clusters in optic nerves from eyes at d7 after intravitreal injections, injected as indicated in (A). SMI-32$^+$ clusters in the NMDA-treated eye were normalized to the PBS control eye from the same animal. n = 6. (H) Quantification of RGCs at d1 after intravitreal injections of PBS, NMDA, rGFP, or rGFP+NMDA. Two-way ANOVA, Bonferroni's *post hoc* test. n = 6. PBS versus NMDA (sham), p = 0.0013; PBS versus NMDA (rVEGFD), p = 0.0059; sham versus rVEGFD (PBS), p > 0.9999; sham versus rVEGFD (NMDA), p = 0.8657. (I) Quantification of RGCs at d7 after intravitreal injections, injected as indicated in (H). Two-way ANOVA, Bonferroni's *post hoc* test. n = 6. PBS versus NMDA (sham), p < 0.0001; PBS versus NMDA (rGFP), p < 0.0001; sham versus rGFP (PBS), p > 0.9999; sham versus rGFP (NMDA), p > 0.9999. (J) Quantification of RGCs at d7 after intravitreal injections, injected as indicated in (H). RGC numbers in the

(legend continued on next page)

completely lost (Figures 8A, 8B, and 8D). In rAAV-shSCR-injected mice, rVEGFD still interfered with formation of empty sleeves (Figures 8E–8G). In rAAV-shVEGFR3-injected mice, however, ECs were no longer protected from the NMDA-triggered degeneration by the administration of rVEGFD, although rVEGFD could activate endothelial VEGFR3 (Figures 8E–8H). Thus, our data indicate that VEGFD-mediated safeguard of RGCs and capillaries from damage takes place by VEGFD directly exerting its protective functions on RGCs and, as a consequence of this phenomenon, sparing ECs from degeneration (Figure 8I).

DISCUSSION

In this study, we found that an injury to RGCs triggers downregulation of neuronal VEGFD and is followed by capillary damage. Moreover, we demonstrate that VEGFD supplementation promotes RGC survival, which is crucial to prevent the formation of collapsed, acellular capillaries. Taken together, VEGFD might have clinical relevance to robustly promote neuronal and vascular integrity.

Degeneration of neurons and regression of capillaries have been reported for several CNS disorders.[4,59] Noxious NMDAR-mediated excitotoxicity has been put forward as a possible cause for many disorders of the CNS.[60–62] Also for pathologies of the visual system, excitotoxic death of neurons, along with damage to the microvasculature, has been described;[8,10] however, no detailed description of the possible influence of neurons on EC integrity is available. In this study, we detected RGC damage after a single intravitreal NMDA injection within 6 h from delivering the insult, which did not significantly progress over time. Degeneration of ECs followed neuronal death temporally. Unlike the widely acknowledged contribution of vascular abnormalities to neurodegeneration,[63] delayed damage to the microvasculature following neural degeneration has been less discussed although it has been observed, for instance, in diabetes and glaucoma.[7,64] Our data suggest that signals deriving from degenerating RGCs might be the cause of capillary damage. Such a hypothesis is further supported by our observations that a direct NMDA insult to cultured brain ECs did not affect their survival, although they express different GluN subunits, ensuring a functional NMDAR.[39,65] An open question remains which nature of signals might carry the message that RGCs are degenerating to the ECs. This process might be ascribed to an imbalance in the expression of particular factors and could involve multiple cell types. In this view, it is appealing to speculate that the reduction of VEGFD levels in RGCs, which we detected, might be playing a role; however, such a hypothesis calls for future in-depth investigations.

Of the several parameters measured, including expression of markers and functionality of the BRB as well as detailed analysis of the microvascular architecture, we only observed alterations in the increased presence of string vessels as a consequence of injured RGCs. Our data therefore suggest that EC damage is not necessarily correlated to BRB disruption. BRB breakdown might be staggered in time or uncoupled, a phenomenon that has been previously observed.[30,66] Mechanistically, a possible explanation may be that the affected capillaries would collapse and stop being perfused before leakage and disruption could take place.[67]

Neurons can influence the vascular system in different ways. While synaptic activity drives vascular patterning during CNS development, neural cells provide feedback to vessels regarding their metabolic needs in the mature brain, allowing regional adjustments of blood flow in response to changing neuronal activity.[1,68] Our study showed for the first time that damaged neurons could have a noxious impact on the vasculature. In addition, we provide information on the possible causes driving the formation of empty sleeves, a phenomenon largely uncharacterized and unexplained. Empty sleeves can be present in low number in physiological conditions, but their number dramatically increases throughout the CNS during aging and in neurodegenerative diseases such as diabetic retinopathy, Alzheimer's disease, stroke, glaucoma, and Parkinson's disease.[69–72] Our data point toward the idea that structural and functional integrity of neurons is critical for the maintenance of healthy capillaries and that, when neurons are compromised or damaged, this negatively affects ECs. The resulting creation of collapsed capillaries might in turn exacerbate neurodegeneration and create a vicious circle of vascular and neural dysfunctions. Future work needs to extend our findings obtained with an acute tool to promote RGC degeneration to different models of CNS disorders and to different brain regions.

Interestingly, among the members of the VEGF family and their receptors, known key modulators of neurovascular communication,[3–6] our study identified VEGFD as the only one whose expression in the retina was affected by the excitotoxic insult to RGCs. Such observations are in agreement with our recent findings showing that VEGFD expression, but not that of other VEGFs or VEGFRs, is shut off following toxic activation of NMDARs in pyramidal neurons *in vitro* or *in vivo* following stroke (D.M., B. Buchthal, T.J. Hemstedt, U. Weiss, C.D. Klein, and H. Bading, unpublished data). Several factors, such as synaptic activity, nuclear calcium signaling, and epigenetic regulators, can modulate VEGFD expression in neurons while leaving expression of VEGFC, VEGF, and VEGFRs unaltered,[43,51] thus suggesting that VEGFD neuronal expression is under a peculiar and dynamic regulation. In this study, we showed for the first time that VEGFD is expressed in RGCs in the human retina, and we found that the NMDA-triggered downregulation of VEGFD is taking place specifically in RGCs and not in other cell types of

NMDA-treated eye were normalized to the PBS control eye from the same animal. n = 6. (K) Quantification of SMI-32$^+$ clusters in optic nerves at d7 after intravitreal injections, injected as indicated in (H). Two-way ANOVA, Bonferroni's *post hoc* test. n = 5. PBS versus NMDA (sham), p = 0.0036; PBS versus NMDA (rGFP), p = 0.0041; sham versus rGFP (PBS), p > 0.9999; sham versus rGFP (NMDA), p > 0.9999. (L) Quantification of SMI-32$^+$ clusters in optic nerves from eyes at d7 after intravitreal injections, injected as indicated in (H). SMI-32$^+$ clusters in the NMDA-treated eye were normalized to the PBS control eye from the same animal. n = 6. Bars represent mean ± SEM. Dots represent single values. **p < 0.01, ***p < 0.001, ****p < 0.0001. See also Figure S2.

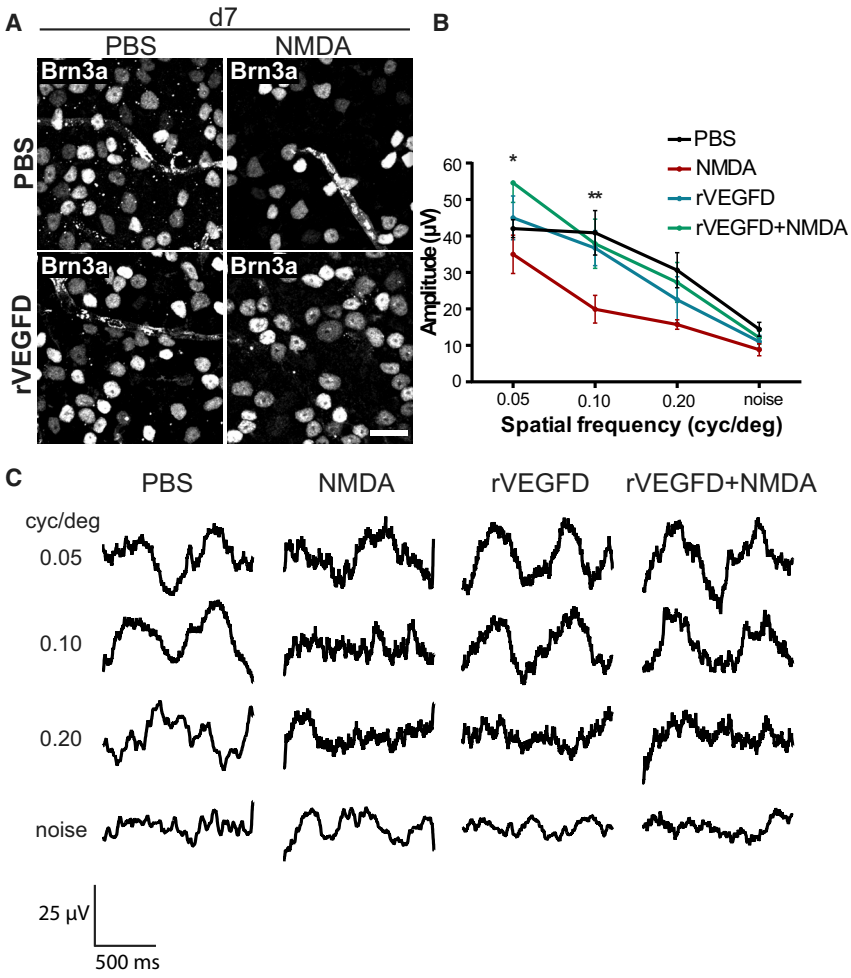

Figure 6. Recombinant VEGFD Prevents Decrease of Pattern Electroretinography Amplitudes after NMDA-Triggered Damage to RGCs

(A) Representative images of retinal whole mounts at d7 after intravitreal injections of PBS, NMDA, rVEGFD, or rVEGFD+NMDA. RGCs were immunolabeled against Brn3a. Scale bar, 20 μm. (B) Amplitude of the second harmonic of the fast Fourier transformation plotted against spatial frequency of stimulation. Asterisks indicate statistical significance between NMDA- and rVEGFD+NMDA-treated animals. Two-way ANOVA, Bonferroni's *post hoc* test. n = 4. PBS versus NMDA (0.05 cyc/deg), p = 0.6877; PBS versus NMDA (0.10 cyc/deg), p = 0.0076; PBS versus NMDA (0.20 cyc/deg), p = 0.0964; PBS versus NMDA (noise), p = 0.8182; PBS versus rVEGFD (0.05 cyc/deg), p = 0.9669; PBS versus rVEGFD (0.10 cyc/deg), p = 0.9140; PBS versus rVEGFD (0.20 cyc/deg), p = 0.5811; PBS versus rVEGFD (noise), p = 0.9509; rVEGFD versus rVEGFD+NMDA (0.05 cyc/deg), p = 0.4433; rVEGFD versus rVEGFD+NMDA (0.10 cyc/deg), p = 0.9976; rVEGFD versus rVEGFD+NMDA (0.20 cyc/deg), p = 0.8797; rVEGFD versus rVEGFD+NMDA (noise), p = 0.9980; NMDA versus rVEGFD+NMDA (0.05 cyc/deg), p = 0.0144; NMDA versus rVEGFD+NMDA (0.10 cyc/deg), p = 0.0296; NMDA versus rVEGFD+NMDA (0.20 cyc/deg), p = 0.2776; NMDA versus rVEGFD+NMDA (noise), p = 0.9980. (C) Representative pattern electroretinography waveforms recorded from mice injected as indicated in (A). Bars represent mean ± SEM. Dots represent single values. *p < 0.05, **p < 0.01.

the neurovascular unit, despite the fact that ECs and astrocytes carry functional NMDARs.[32,40,65,73] Excitotoxicity in the retina alters the subcellular distribution, and thus activity, of the epigenetic regulators histone deacetylases (HDACs) in RGCs.[26] The activity of one particular HDAC, namely HDAC4, regulates the expression of VEGFD.[51] It remains an open question whether such epigenetic regulators are involved in the decrease of VEGFD levels described in the present study.

RGCs lose dendrites before they die due to NMDA-mediated excitotoxicity[74] and in several animal models of excitotoxicity-associated disorders such as glaucoma and optic nerve crush.[75–79] In a mouse model of stroke, a pathology also characterized by excitotoxic mechanisms, VEGFD supplementation, but not VEGFC or VEGFA, spared cortical neurons from stroke-induced damage (D.M., B. Buchthal, T.J. Hemstedt, U. Weiss, C.D. Klein, and H. Bading, unpublished data). This is mechanistically implemented by VEGFD preserving the dendritic connections of cortical neurons, and, as a result, preventing neurodegeneration (D.M., B. Buchthal, T.J. Hemstedt, U. Weiss, C.D. Klein, and H. Bading, unpublished data). Here, using different approaches, we uncovered the protective functions of VEGFD on both the degenerating neural and vascular components of the retina. It is highly likely that the detected beneficial effects of VEGFD on RGCs, as happens for pyramidal neurons, may be due to the specific properties of VEGFD to preserve and maintain dendritic connections.[43,49–51] In recent years, rAAVs received increasing attention as tools for gene delivery for the treatment of several diseases.[80,81] For eye diseases, in particular, they are already under investigation in clinical trials and rapidly approaching medical praxis.[81] We first used rAAVs to boost the production of VEGFD in RGCs without affecting VEGFD expression in other cell types. This approach significantly blunted the excitotoxic damage to RGCs, optic nerve axons, and the microvasculature. Even if we did not detect any effects as a result of the sole overexpression of VEGFD in absence of the toxic insult, we cannot completely rule out that some additional mechanisms owing to the long-term expression of VEGFD might be participating in the protective effects. Notably, however, acute VEGFD treatment via intravitreal injections of the mature form of VEGFD (rVEGFD) recapitulated the same protective properties achieved via rAAV-mediated neuronal VEGFD overexpression. Moreover, rVEGFD administration also restored the impaired functionality of RGCs following excitotoxicity. As RGCs are responsible for transmitting visual information to the brain and their death is accompanied by devastating effects on vision,[82]

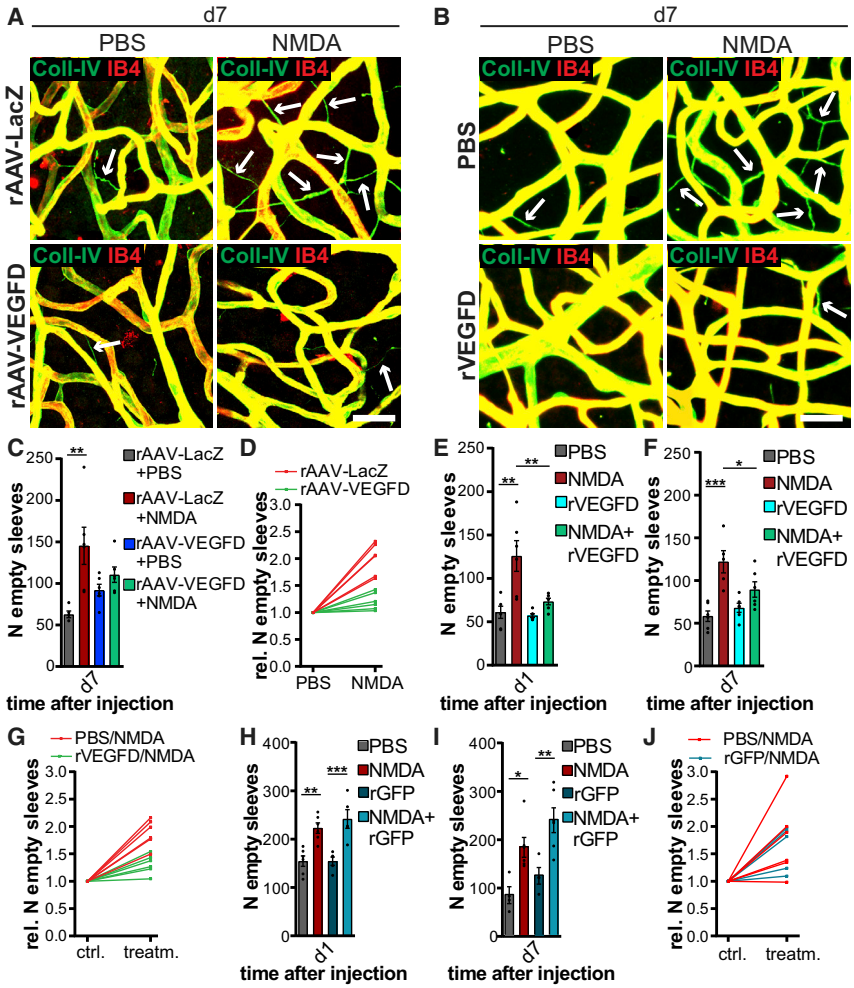

Figure 7. VEGFD Reduces Formation of Empty Sleeves Triggered by Intravitreal NMDA Injection

(A) Representative images of retinal whole mounts at d7 after intravitreal injections of NMDA or PBS from mice injected either with rAAV-LacZ or rAAV-VEGFD as indicated. Vessels were immunolabeled against collagen IV (Coll-IV, green) and using isolectin B4 (IB4, red). Scale bar, 30 μm. (B) Representative images of retinal whole mounts at d7 after intravitreal injections of PBS, NMDA, rVEGFD, or rVEGFD+NMDA. Vessels were immunolabeled against collagen IV (Coll-IV, green) and using isolectin B4 (IB4, red). Scale bar, 30 μm. (C) Quantification of empty sleeves at d7 after intravitreal injections, injected as indicated in (A). Two-way ANOVA, Bonferroni's *post hoc* test. n = 6. rAAV-LacZ+PBS versus rAAV-LacZ+NMDA, p = 0.0008; rAAV-VEGFD+PBS versus rAAV-VEGFD+NMDA, p = 0.6565; rAAV-LacZ+PBS versus rAAV-VEGFD+PBS, p = 0.2950; rAAV-LacZ+NMDA versus rAAV-VEGFD+NMDA, p = 0.1484. (D) Quantification of empty sleeves at d7 after intravitreal injections, injected as indicated in (A). Number of empty sleeves in the NMDA-treated eye was normalized to the PBS control eye from the same animal. n = 6. (E) Quantification of empty sleeves at d1 after intravitreal injections with PBS, NMDA, rVEGFD, or rVEGFD+NMDA. Two-way ANOVA, Bonferroni's *post hoc* test. n = 6. PBS versus NMDA (sham), p = 0.0003; PBS versus NMDA (rVEGFD), p = 0.5067; sham versus rVEGFD (PBS), p > 0.9999; sham versus rVEGFD (NMDA), p = 0.0022. (F) Quantification of empty sleeves at d7 after intravitreal injections, injected as indicated in (B). Two-way ANOVA, Bonferroni's *post hoc* test. n = 6. PBS versus NMDA (sham), p = 0.0001; PBS versus NMDA (rVEGFD), p = 0.1673; sham versus rVEGFD (PBS), p = 0.8438; sham versus rVEGFD (NMDA), p = 0.0329. (G) Quantification of empty sleeves at d7 after intravitreal injections, injected as indicated in (B). Number of empty sleeves in the NMDA-treated eye was normalized to the PBS control eye from the same animal. n = 6. (H) Quantification of empty sleeves at d1 after intravitreal injections of PBS, NMDA, rGFP, or rGFP+NMDA. Two-way ANOVA, Bonferroni's *post hoc* test. n = 6. PBS versus NMDA (sham), p = 0.0019; PBS versus NMDA (rGFP), p = 0.0004; sham versus rGFP (PBS), p > 0.9999; sham versus rGFP (NMDA), p = 0.6279. (I) Quantification of empty sleeves at d7 after intravitreal injections, injected as indicated in (H). Two-way ANOVA, Bonferroni's *post hoc* test. n = 6. PBS versus NMDA (sham), p = 0.0143; PBS versus NMDA (rGFP), p = 0.0050; sham versus rGFP (PBS), p = 0.5439; sham versus rGFP (NMDA), p = 0.1376. (J) Quantification of empty sleeves at d7 after intravitreal injections, injected as indicated in (H). Number of empty sleeves in the NMDA-treated eye was normalized to the PBS control eye from the same animal. n = 6. Graphs represent mean ± SEM. *p < 0.05, **p < 0.01, ***p < 0.001. See also Figure S1.

therapies designed to promote survival of RGCs are of the utmost relevance. Our work highlights the possible therapeutic capacity of VEGFD supplementation to treat vision deficiency associated with RGC degeneration.

Our results revealed that, in addition to protecting the neural components of the retina, VEGFD prevented the formation of empty sleeves. These findings might be interpreted as a possible direct mechanism of VEGFD on ECs, sparing them from degeneration. However, multiple evidences argue against this line of thought. First, our data indicate that in our model empty sleeve formation follows RGC damage and that VEGFD levels in ECs are not affected by the insult. Although rAAV-mediated neuronal overexpression of VEGFD would increase the levels of available VEGFD free to act on both RGCs and ECs, as the overexpressed protein undergoes proteolytic maturation and is secreted,[43] VEGFD acts primarily via an autocrine mechanism in neurons[43] as well as in other cell types.[83–86] Thus, it is probable that VEGFD produced by RGCs would act primarily on autocrine receptors of RGCs, protecting them from NMDA-mediated damage and, consequently, preventing the formation of empty sleeves. The most conclusive piece of evidence, however, derives from our observations that decreasing VEGFR3 expression specifically in RGCs prevents the VEGFD-mediated protection of RGCs, and, as a result, leads also to loss of protection of ECs.

In conclusion, an insult specifically targeting RGCs is accompanied by a reduction of VEGFD levels in RGCs and, eventually, by damage to the capillaries. Boosting VEGFD levels protects the structure and function of RGCs from the injury and, as a result, spares the capillaries from degeneration. Our findings about the VEGFD-mediated

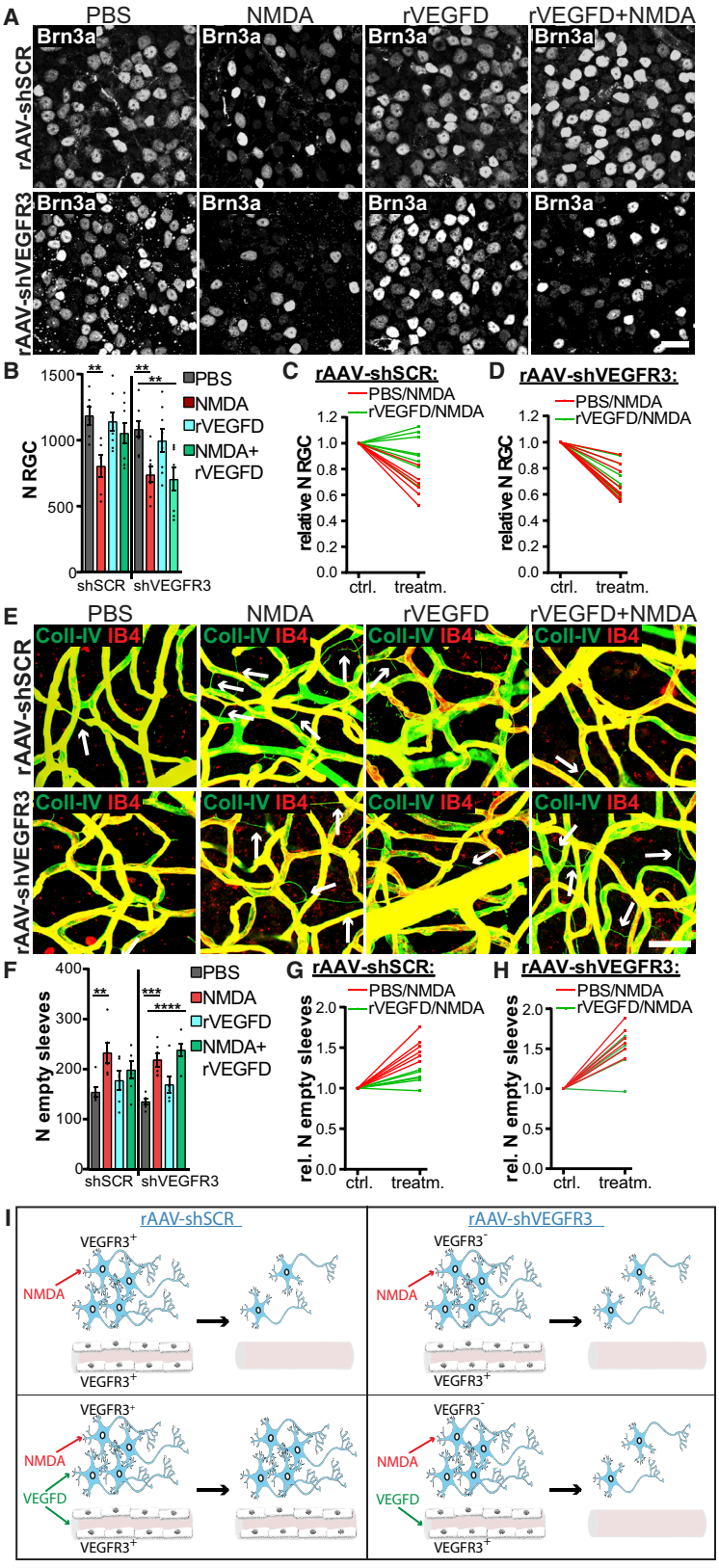

Figure 8. VEGFD Protection against NMDA-Triggered Excitotoxic Retinal Damage Is Mediated by Neuronal VEGFR3 Expression

(A) Representative confocal scans of retinal whole mounts at d7 after intravitreal injections of PBS, NMDA, rVEGFD, or rVEGFD+NMDA from mice intravitreally injected either with rAAV-shSCR (control) or rAAV-shVEGFR3. RGCs were immunolabeled using Brn3a. Scale bar, 20 μm. (B) Quantification of RGCs injected as indicated in (A). Two-way ANOVA, Bonferroni's *post hoc* test. n = 8. rAAV-shSCR+PBS versus rAAV-shSCR+NMDA, p = 0.0067; rAAV-shSCR+PBS versus rAAV-shSCR+rVEGFD, p = 0.9583; rAAV-shSCR+PBS versus rAAV-shSCR+rVEGFD+NMDA, p = 0.4943; shVEGFR3+PBS versus rAAV-shVEGFR3+NMDA, p = 0.0046; rAAV-shVEGFR3+PBS versus rAAV-shVEGFR3+rVEGFD, p = 0.7359; rAAV-shVEGFR3+PBS versus rAAV-shVEGFR3+rVEGFD+NMDA, p = 0.0017. (C) Quantification of RGCs at d7 after intravitreal injections, injected as indicated in (A), in rAAV-shSCR-injected eyes. RGC numbers in the NMDA-treated eye were normalized to the PBS control eye from the same animal. n = 8. (D) Quantification of RGCs at d7 after intravitreal injections injected as indicated in (A), in rAAV-shVEGFR3-injected eyes. RGC numbers in the NMDA-treated eye were normalized to the PBS control eye from the same animal. n = 8. (E) Representative confocal scans of retinal whole mounts at d7 after intravitreal injections of PBS, NMDA, rVEGFD, or rVEGFD+NMDA from mice injected either with rAAV-shSCR or rAAV-shVEGFR3 as indicated. Vessels were immunolabeled using collagen IV (Coll-IV, green) and isolectin B4 (IB4, red). Scale bar, 30 μm. (F) Quantification of empty sleeves injected as indicated in (E). Two-way ANOVA, Bonferroni's *post hoc* test. n = 6. rAAV-shSCR+PBS versus rAAV-shSCR+NMDA, p = 0.0018; rAAV-shSCR+PBS versus rAAV-shSCR+rVEGFD, p = 0.5622; rAAV-shSCR+PBS versus rAAV-shSCR+rVEGFD+NMDA, p = 0.1073; rAAV-shVEGFR3+PBS versus rAAV-shVEGFR3+NMDA, p = 0.0009; rAAV-shVEGFR3+PBS versus rAAV-shVEGFR3+rVEGFD, p = 0.2623; rAAV-shVEGFR3+PBS versus rAAV-shVEGFR3+rVEGFD+NMDA, p = 0.0001. (G) Quantification of empty sleeves at d7 after intravitreal injections, injected as indicated in (E), in rAAV-shSCR-injected eyes. Number of empty sleeves in the NMDA-treated eye was normalized to the PBS control eye from the same animal. n = 8. (H) Quantification of empty sleeves at d7 after intravitreal injections, injected as indicated in (E), in rAAV-shVEGFR3-injected eyes. Number of empty sleeves in the NMDA-treated eye was normalized to the PBS control eye from the same animal. n = 8. (I) Schema of neuronal-mediated VEGFD protection against excitotoxic retinal damage. Upper row, left panel: NMDA triggers RGC and EC degeneration in rAAV-shSCR-injected mice by direct action on RGCs (red arrows). RGCs and ECs express VEGFR3 (VEGFR3$^+$). Lower row, left panel: VEGFD prevents RGCs and ECs from NMDA-triggered degeneration in rAAV-shSCR-injected mice. RGCs and ECs express VEGFR3 (VEGFR3$^+$). VEGFD can act on VEGFR3 in both RGCs and ECs (green arrows). Upper row, right panel: NMDA triggers RGC and EC degeneration in rAAV-shVEGFR3-injected mice by direct action on RGCs (red arrows). RGCs do not express VEGFR3 (VEGFR3$^-$); ECs express VEGFR3 (VEGFR3$^+$). Lower row, right panel: In rAAV-shVEGFR3-injected mice, VEGFD does not prevent RGCs and ECs from NMDA-triggered degeneration. RGCs do not express VEGFR3 (VEGFR3$^-$); ECs express VEGFR3 (VEGFR3$^+$). VEGFD cannot act on VEGFR3 in RGCs, but on VEGFR3 in ECs (green arrows). Graphs represent mean ± SEM. **p < 0.01, ***p < 0.001, ****p<0.0001 See also Figure S1.

prevention of RGC loss and capillary damage is particularly interesting in light of potential clinical applications targeting CNS diseases in which dysfunctions of the neurovascular system have been implicated. Strategies aiming at enhancing neuronal and capillary survival through VEGFD supplementation may therefore represent approaches for the development of therapies for age- and disease-related dysfunctions of the neurovascular system.

MATERIALS AND METHODS

Animals

All experiments were performed in accordance with ethics guidelines imposed by the local governing body (Regierungspräsidium Karlsruhe, Germany). Adult 8-week-old male mice of the strain C57BL/6J (Charles River, Sulzfeld, Germany) were used in this study. Mice were housed in groups of a maximum of four animals in the animal facility at the Heidelberg University in standard cages (15 × 21 × 13.5 cm) on a normal 12-h light/12-h dark cycle with *ad libitum* access to water and food. Each cage contained nesting material. Animals were randomly allocated to treatment groups. After intravitreal injections, mice were kept under frequent observation to ensure animal welfare.

Human Retina Samples

All eyes used in this study were taken under the legal responsibility of the Department of Ophthalmology, Lions Eye Bank (Federal authority Paul Ehrlich Institute: PEI.G.11601.01.1), within the facilities of the University Hospital Heidelberg for the purpose of cornea transplantation. Human retina samples were obtained from two cornea donations within 48 h of death after cornea trephination. Informed consent of relatives to use the tissues for scientific purposes was present for all eyes used in this study.

Intravitreal Injections of Chemicals and Proteins

For intravitreal injections, mice were anesthetized by intraperitoneal injection of 0.3 mg/kg body weight (BW) medetomidine (Alvetra und Werfft, Vienna, Austria), 3 mg/kg BW midazolam (Hameln Pharmaceuticals, Hameln, Germany), and 0.03 mg/kg BW fentanyl (Janssen Pharmaceutica, Beerse, Belgium) to induce deep anesthesia. To induce excitotoxicity in the retina, 10 nmol of NMDA (1 μL of 10 mM, dissolved in sterile 1× PBS; Biotrend, Wangen/Zurich, Switzerland) was injected in one eye with a 32-gauge needle (NanoFil syringe, 10 μL; World Precision Instruments, Sarasota, FL, USA) under a stereomicroscope. The other eye received the same volume of 1× PBS (vehicle) as a control. After the injection, eyes were treated with eye ointment (Bepanthen; Roche, Basel, Switzerland). Afterward, anesthesia was antagonized by 450 μg/kg BW atipamezole (Prodivet Pharmaceuticals, Raeren, Belgium), 0.3 mg/kg BW flumazenil (Fresenius Kabi, Bad Homburg, Germany), and 0.7 mg/kg BW narcanti/naloxone (Inresa Arzneimittel, Freiburg, Germany). For rVEGFD treatment, 100 ng of recombinant mouse VEGFD (1 μL of 100 ng/μL, dissolved in sterile 1× PBS; 469-VD-025/CF; R&D Systems, Minneapolis, MN, USA) was co-injected with PBS or NMDA. Control experiments were performed using 100 ng of recombinant green fluorescent protein (rGFP; 1 μL of 100 ng/μL, dissolved in sterile 1× PBS; recombinant *A. victoria* GFP protein, ab116434, Abcam, Cambridge, UK) was co-injected with PBS or NMDA.

Intravitreal Injections of rAAVs

2 μL of rAAVs was intravitreally injected prior to the excitotoxic insult. To determine efficient duration of protein expression after transduction, protein products were analyzed via western blot of retinal lysates. For rAAV-LacZ and rAAV-VEGFD, incubation of 14 days was sufficient to detect expression, whereas for rAAV-shSCR and rAAV-shVEGFR3 an incubation of 21 days prior to the insult was necessary. Typical infection rate of the employed rAAV range was >60% of $Brn3a^+$ RGCs.

Tissue Preparation

Retinas from mice were dissected 6 h, 1 day (d1), or 7 days (d7) after intravitreal injections. For quantitative reverse transcriptase (qRT-PCR) analysis and western blot, animals were euthanized with CO_2; animals were decapitated and heads were cooled in iced water. For histology, animals were euthanized by intraperitoneal injection with 400 mg/kg BW pentobarbital (Narcoren; Merial, Hallbergmoos, Germany), followed by a transcardial perfusion with ice-cold 1× PBS and 10% formalin for 5 min. Eyes were enucleated and post-fixed for 15 min. In order to dissect the retina, the cornea, iris, lens, and vitreous body were removed under a stereomicroscope. For the preparation of sagittal retina sections, the retina was kept in the surrounding sclera and pigment epithelium. Samples were embedded in Tissue-Tek (Leica, Wetzlar, Germany), frozen, and stored at −80°C until cryo-sectioning. For retina whole-mount immunostainings, the retina was isolated from the sclera and pigment epithelium and transferred into PBS. Human retina samples were dissected and shock-frozen in liquid nitrogen for qRT-PCR analysis or post-fixed for 15 min in 10% formalin for whole-mount immunostainings.

Cryo-Sectioning

Sagittal retina sections of 16-μm and optic nerve sections of 10-μm thickness were obtained with a Leica CM1950 cryostat (Leica) and mounted on Superfrost Plus slides (Thermo Scientific, Waltham, MA, USA). Slides were stored at −20°C until analysis.

TUNEL Assay

TUNEL staining was done on retinal sections on microscope slides. Sections were permeabilized in 0.1% sodium citrate and 0.5% Triton X-100 for 30 min at room temperature and incubated with TUNEL solution for 1 h at 37°C using an *In Situ* Cell Death Detection Kit, TMR red (Roche, Basel, Switzerland). Nuclei were labeled with Hoechst (1:6,000 in 1× PBS; Serva Electrophoresis, Heidelberg, Germany) for 10 min.

Immunohistochemistry

Retinal sections were immunostained directly on microscope slides. Slides were incubated in 0.5% Triton X-100 and 10% fetal calf serum (FCS) in 1× PBS for 1.5 h at room temperature. Primary antibodies were diluted in blocking solution and incubated overnight at 4°C in a humidified chamber. For retinal whole mounts, free-floating

immunostaining was performed. Retinas were blocked in 1% Triton X-100 and 10% FCS in 1× PBS overnight at 4°C. Primary antibodies were diluted in blocking solution and incubated overnight at room temperature. The following antibodies were used: mouse anti-Brn3a (1:500; sc-8429, Santa Cruz Biotechnology, Dallas, TX, USA), rabbit anti-collagen IV (1:500; 2150-1470, Bio-Rad Laboratories, Hercules, CA, USA), mouse anti-VEGFD (1:100; sc-373866, Santa Cruz Biotechnology), mouse-anti Neurofilament H (NF-H), Nonphosphorylated (SMI-32, 1:1,000; 801802, BioLegend, San Diego, CA, USA), mouse anti-HA probe (Y-11) (1:500; sc-805, Santa Cruz Biotechnology), rabbit anti-RBPMS (1:250; ab194213, Abcam), rat anti-TER119 (1:200; MAB1125, R&D Systems, Minneapolis, MN, USA). For VEGFD immunostaining, heat-induced epitope retrieval was performed prior to blocking by incubating the slides in pre-heated sodium citrate buffer (10 mM sodium citrate, 0.05% Tween 20, pH 6.0) at 95°C for 10 min. ECs were labeled with Alexa Fluor 488- or 594-conjugated isolectin B4 (1:100; I21411, I21413, Life Technologies, Carlsbad, CA, USA). The following secondary antibodies were used: goat anti-rabbit IgG (H+L) Alexa Fluor 488 (1:1,000; A11008, Life Technologies), goat anti-mouse IgG (H+L) Alexa Fluor 594 (1:1,000; A11005, Life Technologies), and donkey anti-rat IgG (H+L) Alexa Fluor 488 (1:700; A21208, Life Technologies). Nuclei were labeled with Hoechst (1:6,000 in 1× PBS; Serva Electrophoresis, Heidelberg, Germany) for 10 min.

Transmission Electron Microscopy (TEM)

Mice were transcardially perfused with 2.5% glutaraldehyde/2% polyvidone 25 in 0.1 M sodium phosphate buffer (pH 7.4). The eyes were enucleated and the retinas were dissected as described in the "Tissue Preparation" section above. The tissue was processed for TEM as previously published.[87,88] Retinas were post-fixed with 1% OsO_4 and 1.5% $K_4Fe(CN)_6$, contrasted *en bloc* with uranyl acetate, dehydrated with a graded dilution series of ethanol, and embedded into glycid ether 100-based resin. Ultrathin retinal cross-sections of 85 nm were cut with a Reichert Ultracut S ultramicrotome (Leica Microsystems) and contrasted with uranyl acetate and lead citrate. Sections were examined in an electron microscope (Zeiss EM 10 CR) at an acceleration voltage of 60 kV. The representative electron microscopy images were derived from the same mouse, but two mice were prepared for analysis.

bEnd.3 Cells

bEnd.3 cells were cultured in high-glucose-containing (4.5 g/L) Dulbecco's modified Eagle's medium (DMEM; Life Technologies, Carlsbad, CA, USA) supplemented with 10% fetal bovine serum (FBS), 100 U/mL penicillin, and 100 µg/mL streptomycin (Sigma, Kawasaki, Kanagawa, Japan) on 0.1% gelatin-coated flasks. For passaging, cells were washed with PBS and incubated with trypsin (#25300-054; Gibco, Life Technologies, Carlsbad, CA, USA) for 3 min. Cells were resuspended in medium and centrifuged at 800 × *g* for 3 min. The cell pellet was resuspended in cell culture medium and cells were seeded at an appropriate dilution according to their growth rate. For the bEnd.3 mortality assay, cells were treated with 20 µM NMDA or 1 mM NMDA for 10 min and 24 h. Untreated cells served as controls. After 24 h, cells were fixed for 10 min with 4% paraformaldehyde (PFA) and labeled with Hoechst for cell survival analysis. Hoechst-labeled cells were automatically counted in 16 images out of four coverslips using a self-written macro in ImageJ/Fiji. Healthy nuclei were differentiated from fragmented or condensed nuclei by their morphology.

Primary Astrocyte Cultures

Neurons and glial cells from newborn C57BL/6N mice were isolated as described.[49] Medium was changed after 2.5 h from plating with DMEM supplemented with 10% FCS and penicillin/streptomycin. Every 3 days, cultures were washed with ice-cold PBS, to promote death and detachment of neuronal cells, and growth of astrocytes. When confluence was reached, experiments were performed. Cultures were treated for 24 h with 20 µM NMDA and then either harvested for qRT-PCR analysis or fixed for immunocytochemistry. We confirmed the exclusive presence of glia cells using the marker glial fibrillary acidic protein (GFAP; 1:500; 3670, Cell Signaling Technology, Danvers, MA, USA). Hoechst labeling was used to count and assess cellular vitality via nuclear morphology.

rAAVs

The method used to construct, package, and purify rAAVs has been previously described.[89,90] rAAV serotypes 1/2 were produced by co-transfection of HEK293 cells by standard calcium phosphate precipitation. Before transfection, culture medium was replaced with fresh modified Dulbecco's medium (Iscove's modified Dulbecco's medium; Life Technologies, Carlsbad, CA, USA) containing 5% FBS without antibiotics. Packaging of rAAVs was carried out with helper plasmids pFΔ6, pRV1, and pH21 together with pAAV-VEGFD, pAAV-LacZ, pAAV-shVEGFR3, or pAAV-shSCR. After transfection, the medium was replaced with fresh DMEM containing 10% FBS and antibiotics. Cells were collected at low-speed centrifugation, resuspended in 150 mM NaCl/10 mM Tris-HCl (pH 8.5) and lysed by incubation with 0.5% sodium deoxycholate followed by freeze-thaw cycles. rAAVs were purified using heparin affinity columns (HiTrap Heparin HP; GE Healthcare, Chicago, IL, USA). rAAV stocks were concentrated using Amicon Ultra-4 centrifugal filter devices (Merck Millipore, Burlington, MA, USA).

The rAAVs used in this work have been previously extensively characterized *in vitro* and *in vivo* for their specificity and efficacy.[43,50,51] rAAV-VEGFD and rAAV-LacZ carry an HA- or FLAG-tag, respectively, allowing for detection of infected cells. rAAV-shVEGFR3 and rAAV-shSCR carry an additional cassette for mCherry expression for rapid and specific detection of the infected cells. The transduction efficiency was calculated as the percentage of $Brn3a^+$ cells also positive for the transgene expression. The virus batches used for the experiments had a titer of rAAV-LacZ (6×10^{11} molecules/mL)/rAAV-VEGFD (3×10^{11} molecules/mL), which had, however, identical infection efficiency in both cultured neurons and *in vivo* in RGCs. For the shRNA constructs, the virus batches used for the experiments had a titer of rAAV-shSCR (6×10^{12} molecules/ml)/rAAV-shVEGFR3 (2×10^{12} molecules/mL), which had, however, identical infection efficiency in both cultured neurons and *in vivo* in RGCs.

The number of mice and eyes injected with rAAV-LacZ were 9 mice/18 eyes (9 eyes were injected with PBS, 9 eyes were injected with NMDA, and of each experimental group 6 eyes were co-stained for RGC and empty sleeves quantification while 3 eyes were co-stained only for RGC quantification). The number of mice and eyes injected with rAAV-VEGFD were 9 mice/18 eyes (9 eyes were injected with PBS, 9 eyes were injected with NMDA, and of each experimental group 6 eyes were co-stained for RGC and empty sleeves quantification while 3 eyes were co-stained only for RGC quantification). The number of mice and eyes treated with rAAV-shSCR were 16 mice/32 eyes for quantification of RGC survival (8 eyes were injected with PBS, 8 eyes were injected with NMDA, 8 eyes were injected with rVEGFD, and 8 eyes were injected with NMDA+rVEGFD) and 12 mice/24 eyes for empty sleeves analysis (6 eyes were injected with PBS, 6 eyes were injected with NMDA, 6 eyes were injected with rVEGFD, and 6 eyes were injected with NMDA+rVEGFD). The number of mice and eyes treated with rAAV-shVEGFR3 were 16 mice/32 eyes for quantification of RGC survival (8 eyes were injected with PBS, 8 eyes were injected with NMDA, 8 eyes were injected with rVEGFD, and 8 eyes were injected with NMDA+rVEGFD) and 12 mice/24 eyes for empty sleeves analysis (6 eyes were injected with PBS, 6 eyes were injected with NMDA, 6 eyes were injected with rVEGFD, and 6 eyes were injected with NMDA+rVEGFD).

qRT-PCR

Total RNA was extracted from bEnd.3 cells, primary astrocytes, and mouse or human retinas using the RNeasy Mini Kit (QIAGEN, Hilden, Germany) including an optional DNase I treatment at room temperature for 15 min according to the manufacturer's instructions (QIAGEN). Extracted RNA was reverse transcribed into first-strand cDNA using a high-capacity cDNA reverse transcription kit (Applied Biosystems, Foster City, CA, USA). qRT-PCR was performed on a StepOne Plus real-time PCR system using TaqMan gene expression assays for the indicated genes (Applied Biosystems). The following TaqMan gene expression assays were used in this study: *Thy1* (Mm01174153_m1), *nefl* (Mm01315666_m1), *ocld* (Mm01282968_m1), *cld5* (Mm00727012_m1), *tjp1* (Mm00493699_s1), *vegfd* (Mm00438963_m1), *vegfc* (Mm01202432_m1), *vegf* (Mm01281449_m1), *flt4* (Mm01292618_m1), *flt1* (Mm00438980_m1), and *kdr* (Mm00440099_m1). Expression of target genes was normalized against the expression of *Gapdh* (Mm99999915_g1) or, in the case of bEnd.3 cells, *Gusb* (Mm00446953_m1), which were used as endogenous control genes. For detection of VEGFD in human retina, the following probes were used: *vegfd* (Hs01128659_m1), *vegf* (Hs00900055_m1), and *actb* (Hs99999903_m1). For each treatment, six animals, three technical replicates, or four human retinas from two donors were analyzed.

Western Blot Analysis

bEnd.3 cells were homogenized in RIPA buffer (150 mM NaCl, 1% Triton X-100, 0.57% sodium deoxycholate, 0.1% SDS, 50 mM Tris [pH 8], 1× Complete cocktail of protease inhibitors; Roche, Basel, Switzerland). Homogenates were centrifuged at 13,000 rpm for 10 min. Supernatants were mixed with 4× Laemmli sample buffer (200 mM Tris/HCl [pH 6.8], 8% SDS, 40% glycerol, 50 mM EDTA, 0.08% bromophenol blue) and 1% dithiothreitol. Lysates were heated at 95°C for 10 min before performing standard SDS-PAGE and western blotting. The following primary antibodies were used: rabbit anti-GAPDH (1:20,000 in 5% BSA; 2118, Cell Signaling Technology), rabbit anti-GluN1 (1:2,000 in 5% milk; 5704, Cell Signaling Technology), rabbit-GluN2A (1:500 in 5% milk; AB1555, Merck Millipore), rabbit anti-GluN2B (1:1,000 in 5% milk; NB300-106, Novus Biologicals, Centennial, CO, USA), rabbit anti-GluN2C (1:1,000 in 5% milk; PAB9705, Abnova, Taiwan, China), and rabbit anti-GluN2D (1:1,000 in 5% milk; AP21181PU-N, Acris OriGene, Herford, Germany). The following secondary antibody was used: peroxidase AffiniPure goat anti-rabbit IgG (H+L) (1:5,000 in 5% milk; 111-035-144, Jackson ImmunoResearch Laboratories, West Grove, PA, USA). Membranes were developed with enhanced chemiluminescence (ECL) solution (GE Healthcare, Chicago, IL, USA) and the ChemiDoc imaging system (Bio-Rad).

Analysis of BRB Functionality

For extravasation experiments, animals received intravenous injection of fluorescein-conjugated dextran (3 kDa, 50 μg/μL in 1× PBS, 50 μg/g BW; D3306; Thermo Scientific). After 15 min, mice were euthanized by intraperitoneal injection with 400 mg/kg BW pentobarbital (Narcoren; Merial, Hallbergmoos, Germany), followed by a transcardial perfusion with 10 mL of ice-cold 1× PBS to clear the remaining intravascular dextran. A blood sample, serving as positive control, was collected immediately before perfusion. The blood sample was centrifuged at 15,000 × *g* for 5 min at 4°C, and the supernatant was frozen at −20°C until measurements. Blood sera were diluted 1:100 and 1:1,000. Immediately after perfusion, retinas were dissected, weighed, and homogenized in 100 μL of ice-cold 1× PBS. The extracts were centrifuged at 10,000 × g for 15 min at 4°C. The supernatant was kept undiluted or was diluted 1:100. The fluorescence in each 100-μL sample was measured (excitation, 492 nm; emission, 521 nm) using a spectrofluorometer (SpectraMax M5; Molecular Devices, San Jose, CA, USA) with 1× PBS as a blank. Retinal or serum autofluorescence was corrected based on noninjected controls. For normalization, the corrected retinal fluorescence was divided by the retinal weight and by the corrected serum fluorescence, with the results being expressed in relative fluorescence units (RFU).

For extravasation analysis of albumin or IgG via western blotting,[30] animals were euthanized as described above, followed by a transcardial perfusion with 10 mL of ice-cold 1× PBS to reduce blood contaminants. Eyes were enucleated, and retinas were immediately dissected under a stereomicroscope and shock-frozen in liquid nitrogen. Retinas were processed for standard western blot analysis. Western blotting was performed as described above. As controls, recombinant albumin (45 μg; 8076, Roth, Karlsruhe, Germany), mouse IgG (9 μg; sc-2025, Santa Cruz Biotechnology), and retinal lysates from non-perfused animals were loaded. The following primary and secondary antibodies were used to detect endogenous, extravasated albumin and IgG: goat anti-mouse serum albumin (1:1,000; ab19194, Abcam) and peroxidase

AffiniPure goat anti-mouse IgG (H+L) (1:5,000 in 5% milk; 705-035-147, Jackson ImmunoResearch Laboratories). For protein expression analysis, relative protein band densities were calculated by normalizing to the loading control (GAPDH) using ImageJ/Fiji. For each time point d1 and d7, relative protein levels of the NMDA-treated eyes were normalized to relative protein levels of the PBS control eye of the same animal. For all image analyses, backgrounds were subtracted. For each treatment, three animals were analyzed.

Image Acquisition

For each analysis, images were acquired with constant microscopy settings (exposure time, pixel size, bit depth, and binning) across experiments. For fluorescence intensity analysis, all images were acquired on the same day to avoid possible variations in fluorescence lamp excitation. Images of sagittal retina sections and primary astrocytes were acquired with a Leica DM IRBE inverted fluorescent microscope with a 40× oil immersion objective (Leica) and a Spot Insight FireWire 2 camera with VisiView software (Visitron Systems, Diagnostic Instruments, Puchheim, Germany). Images of mouse and human retina whole mounts were acquired with a Nikon A1R confocal laser-scanning microscope (at the Nikon Imaging Center of Heidelberg University, Heidelberg, Germany) with a 63× oil immersion objective (Nikon, Minato, Tokyo, Japan) or with a Leica SP8 confocal laser scanning microscope with a 63× oil immersion objective (Leica).

Quantification of RGCs

For RGC number quantification in retinal whole mounts, $Brn3a^+$ cells were manually counted in eight images per retina equally acquired in the central and peripheral part of the retina using ImageJ/Fiji (see schema Figure 1B). For each eye, RGC number was summed. Relative RGC numbers were calculated by normalizing RGC number in the NMDA-treated eye to the number of RGCs in the PBS-treated eye of the same animal. For each treatment, six animals were analyzed.

INL Analysis

For INL analysis, the thickness of the INL was measured at five different positions across the INL in three sagittal retinal sections of 10-μm thickness using ImageJ/Fiji. For each section, values were averaged and converted into μm taking the microscope resolution into account. For each treatment, three animals were analyzed.

Quantification of Axonal Damage

For axonal damage analysis, the area of $SMI\text{-}32^+$ clusters was quantified in three to four sagittal optic nerve sections of 10-μm thickness using ImageJ/Fiji. For each optic nerve, the cluster area was summed and normalized to the analyzed area. Relative cluster areas were calculated by normalizing the cluster area in the NMDA-treated optic nerve to the cluster area in the PBS-treated optic nerve of the same animal. For each treatment, six animals were analyzed.

Quantification of Vascular Injury

For vascular injury analysis in retinal whole mounts, the number of regressed vessels—so-called empty sleeves, which represent collapsed collagen IV-positive/isolectin B4-negative vessels—was quantified using ImageJ/Fiji. For each eye, the empty sleeves number was summed. Relative empty sleeves numbers were calculated by normalizing the number of empty sleeves in the NMDA-treated eye to the number of empty sleeves in the PBS-treated eye of the same animal. For each treatment, six animals were analyzed.

Quantification of Vessel Architecture

For vessel architecture in retinal whole mounts, the isosurface of collagen IV-immunolabeled vessels was measured with ImageJ/Fiji and the plugin BoneJ. Vessel diameter and length were measured with ImageJ/Fiji and the plugin DiameterJ. Relative values were calculated by normalizing the mean values in the NMDA-treated eye to the mean values in the PBS-treated eye of the same animal. For each treatment, six animals were analyzed.

Analysis of VEGFD expression

Somatic levels of VEGFD in sagittal retinal sections were analyzed as previously published.[26] Fluorescent signals were measured in cells located in the ganglion cell layer by manually drawing regions of interest around the ganglion cell layer in four to five images, each corresponding to one individual 16-μm sagittal retina section using ImageJ/Fiji. For each eye/condition, mean integrated densities were calculated out of the single fluorescence values within each sagittal retinal section. The mean integrated density of the NMDA-treated eye was then normalized to the mean integrated density of the PBS-treated eye of the same animal. Background subtraction was performed prior to all analyses. For negative controls, a blocking peptide (sc-373866, Santa Cruz Biotechnology) was pre-absorbed with the primary antibody in a 5-fold excess (by weight), resulting in the absence of specific immunolabeling of the primary antibody. For each treatment, n = 3–4 animals were analyzed.

Electroretinography

Mice were anaesthetized with ketamine (150 mg/kg; Atarost, Twistringen, Germany) and xylazine (10 mg/kg; Albrecht, Aulendorf, Germany). Electroretinography (ERG) recordings were made using the UTAS visual diagnostic system (LKC Technologies, Gaithersburg, MD, USA) using a contact lens electrode with gold contact (LKC Technologies). The electrical contact, as well as prevention of eye desiccation, was facilitated through application of Liquifilm O.K. (Allergen, Westport, Ireland). Reference and ground needle electrodes were placed subcutaneously in the neck and tail, respectively. A heating pad controlled by a rectal temperature probe was maintained at 37°C. Mice were centered at a distance of 15 cm in front of a 17-inch cathode ray tube monitor. In order to achieve maximum focus of the pattern stimulation, pupils were not dilated. Vertical square-wave grating stimulations (66% contrast, temporal frequency of 1 Hz, equivalent to two pattern reversals per second) were presented at different spatial frequencies (0.05, 0.10, and 0.20 cyc/deg), and noise levels were measured with the monitor turned off. Due to the small amplitudes of pattern ERG, 250 sweeps were averaged to increase the signal-to-noise ratio. Responses were sampled at 1,000×, band-pass filtered between 0.3 and 300 Hz, and amplified

(64× gain). The amplitude of the second harmonic (2 Hz) was analyzed with the fast Fourier transformation function using the EMWin software provided with the UTAS visual diagnostic system.

Statistical Analysis

Mean values and standard error of the mean (SEM) were calculated in Excel (Microsoft), plotted and analyzed in GraphPad Prism 7 software (GraphPad Software). Values were tested for normal distribution by performing a Shapiro-Wilk normality test. An unpaired t test and one-way or two-way analysis of variance (ANOVA) with Bonferroni's *post hoc* test for multiple comparisons were used. Details on the test used and sample size of each experiment are indicated in the respective figure legends. Bars represent mean values. Error bars indicate SEM. Statistical significance is indicated as follows: *$p < 0.05$, **$p < 0.01$, ***$p < 0.001$, ****$p < 0.0001$.

SUPPLEMENTAL INFORMATION

Supplemental Information can be found online at https://doi.org/10.1016/j.omtm.2019.12.009.

AUTHOR CONTRIBUTIONS

Conceptualization, D.M.; Methodology, A.S. and D.M.; Formal Analysis, A.S., B.A., R.F., and D.M.; Investigation, A.S., B.A., R.F, and D.M.; Writing – Original Draft, A.S. and D.M.; Writing – Review & Editing, A.S., B.A., R.F., R.D., and D.M.; Visualization, A.S. and D.M.; Supervision, A.S. and D.M.; Project Administration, D.M., Funding Acquisition, D.M.

CONFLICTS OF INTEREST

D.M. is one of the founders and shareholders of FundaMental Pharma GmbH. The remaining authors declare no competing interests.

ACKNOWLEDGMENTS

The authors wish to thank Dr. Patrick Merz from the Department of Ophthalmology, Lions Eye Bank, Heidelberg University Hospital, for providing human retina samples. The authors are extremely grateful toward Andrea Hellwig for providing the electron microscopy images shown in Figure 2. The authors additionally thank Eva Bindewald and Viktoria Greeck for technical assistance, Iris Bünzli-Ehret and Dr. Anna M. Hagenston for help with the preparation of astrocytic primary cultures, and Dr. Carmen Ruiz de Almodovar for kindly providing the TER119 antibody. D.M. is a member of the Excellence Cluster CellNetworks at Heidelberg University. Selected images were acquired at the Nikon Imaging Center at Heidelberg University. We also acknowledge support from the Interdisciplinary Neurobehavioral Core (INBC) at Heidelberg University. This work was supported by the FOR2325 grant (project 2) and SFB1158 grant (project A08) of the Deutsche Forschungsgemeinschaft (DFG) to D.M., and by the FRONTIER grant of Heidelberg University to D.M.

REFERENCES

1. Paredes, I., Himmels, P., and Ruiz de Almodóvar, C. (2018). Neurovascular communication during CNS development. Dev. Cell *45*, 10–32.
2. Nakahara, T., Mori, A., Kurauchi, Y., Sakamoto, K., and Ishii, K. (2013). Neurovascular interactions in the retina: physiological and pathological roles. J. Pharmacol. Sci. *123*, 79–84.
3. Eichmann, A., and Thomas, J.L. (2013). Molecular parallels between neural and vascular development. Cold Spring Harb. Perspect. Med. *3*, a006551.
4. Quaegebeur, A., Lange, C., and Carmeliet, P. (2011). The neurovascular link in health and disease: molecular mechanisms and therapeutic implications. Neuron *71*, 406–424.
5. Wälchli, T., Wacker, A., Frei, K., Regli, L., Schwab, M.E., Hoerstrup, S.P., Gerhardt, H., and Engelhardt, B. (2015). Wiring the vascular network with neural cues: a CNS perspective. Neuron *87*, 271–296.
6. Okabe, K., Kobayashi, S., Yamada, T., Kurihara, T., Tai-Nagara, I., Miyamoto, T., Mukouyama, Y.S., Sato, T.N., Suda, T., Ema, M., and Kubota, Y. (2014). Neurons limit angiogenesis by titrating VEGF in retina. Cell *159*, 584–596.
7. Zheng, L., Gong, B., Hatala, D.A., and Kern, T.S. (2007). Retinal ischemia and reperfusion causes capillary degeneration: similarities to diabetes. Invest. Ophthalmol. Vis. Sci. *48*, 361–367.
8. Ueda, K., Nakahara, T., Hoshino, M., Mori, A., Sakamoto, K., and Ishii, K. (2010). Retinal blood vessels are damaged in a rat model of NMDA-induced retinal degeneration. Neurosci. Lett. *485*, 55–59.
9. Ueda, K., Nakahara, T., Mori, A., Sakamoto, K., and Ishii, K. (2013). Protective effects of TGF-β inhibitors in a rat model of NMDA-induced retinal degeneration. Eur. J. Pharmacol. *699*, 188–193.
10. Asami, Y., Nakahara, T., Asano, D., Kurauchi, Y., Mori, A., Sakamoto, K., and Ishii, K. (2015). Age-dependent changes in the severity of capillary degeneration in rat retina following *N*-methyl-D-aspartate-induced neurotoxicity. Curr. Eye Res. *40*, 549–553.
11. Brown, W.R. (2010). A review of string vessels or collapsed, empty basement membrane tubes. J. Alzheimers Dis. *21*, 725–739.
12. Catita, J., López-Luppo, M., Ramos, D., Nacher, V., Navarro, M., Carretero, A., Sánchez-Chardi, A., Mendes-Jorge, L., Rodriguez-Baeza, A., and Ruberte, J. (2015). Imaging of cellular aging in human retinal blood vessels. Exp. Eye Res. *135*, 14–25.
13. Hunter, J.M., Kwan, J., Malek-Ahmadi, M., Maarouf, C.L., Kokjohn, T.A., Belden, C., Sabbagh, M.N., Beach, T.G., and Roher, A.E. (2012). Morphological and pathological evolution of the brain microcirculation in aging and Alzheimer's disease. PLoS ONE *7*, e36893.
14. Bading, H. (2017). Therapeutic targeting of the pathological triad of extrasynaptic NMDA receptor signaling in neurodegenerations. J. Exp. Med. *214*, 569–578.
15. Doble, A. (1999). The role of excitotoxicity in neurodegenerative disease: implications for therapy. Pharmacol. Ther. *81*, 163–221.
16. Casson, R.J. (2006). Possible role of excitotoxicity in the pathogenesis of glaucoma. Clin. Exp. Ophthalmol. *34*, 54–63.
17. Dreyer, E.B. (1998). A proposed role for excitotoxicity in glaucoma. J. Glaucoma *7*, 62–67.
18. Dreyer, E.B., Zurakowski, D., Schumer, R.A., Podos, S.M., and Lipton, S.A. (1996). Elevated glutamate levels in the vitreous body of humans and monkeys with glaucoma. Arch. Ophthalmol. *114*, 299–305.
19. Hernández, C., and Simó, R. (2012). Neuroprotection in diabetic retinopathy. Curr. Diab. Rep. *12*, 329–337.
20. Opere, C.A., Heruye, S., Njie-Mbye, Y.F., Ohia, S.E., and Sharif, N.A. (2018). Regulation of excitatory amino acid transmission in the retina: studies on neuroprotection. J. Ocul. Pharmacol. Ther. *34*, 107–118.
21. Sucher, N.J., Lipton, S.A., and Dreyer, E.B. (1997). Molecular basis of glutamate toxicity in retinal ganglion cells. Vision Res. *37*, 3483–3493.
22. Shen, Y., Liu, X.L., and Yang, X.L. (2006). *N*-methyl-D-aspartate receptors in the retina. Mol. Neurobiol. *34*, 163–179.
23. Lebrun-Julien, F., Duplan, L., Pernet, V., Osswald, I., Sapieha, P., Bourgeois, P., Dickson, K., Bowie, D., Barker, P.A., and Di Polo, A. (2009). Excitotoxic death of retinal neurons in vivo occurs via a non-cell-autonomous mechanism. J. Neurosci. *29*, 5536–5545.
24. Li, Y., Schlamp, C.L., and Nickells, R.W. (1999). Experimental induction of retinal ganglion cell death in adult mice. Invest. Ophthalmol. Vis. Sci. *40*, 1004–1008.

25. Nakanishi, N., Tu, S., Shin, Y., Cui, J., Kurokawa, T., Zhang, D., Chen, H.S., Tong, G., and Lipton, S.A. (2009). Neuroprotection by the NR3A subunit of the NMDA receptor. J. Neurosci. *29*, 5260–5265.

26. Schlüter, A., Aksan, B., Fioravanti, R., Valente, S., Mai, A., and Mauceri, D. (2019). Histone deacetylases contribute to excitotoxicity-triggered degeneration of retinal ganglion cells in vivo. Mol. Neurobiol. *56*, 8018–8034.

27. Xiang, M., Zhou, L., Macke, J.P., Yoshioka, T., Hendry, S.H., Eddy, R.L., Shows, T.B., and Nathans, J. (1995). The Brn-3 family of POU-domain factors: primary structure, binding specificity, and expression in subsets of retinal ganglion cells and somatosensory neurons. J. Neurosci. *15*, 4762–4785.

28. Awai, M., Koga, T., Inomata, Y., Oyadomari, S., Gotoh, T., Mori, M., and Tanihara, H. (2006). NMDA-induced retinal injury is mediated by an endoplasmic reticulum stress-related protein, CHOP/GADD153. J. Neurochem. *96*, 43–52.

29. Bartel, H., and Lametschwandtner, A. (2000). Regression of blood vessels in the ventral velum of *Xenopus laevis* Daudin during metamorphosis: light microscopic and transmission electron microscopic study. J. Anat. *197*, 157–166.

30. Ridder, D.A., Wenzel, J., Müller, K., Töllner, K., Tong, X.K., Assmann, J.C., Stroobants, S., Weber, T., Niturad, C., Fischer, L., et al. (2015). Brain endothelial TAK1 and NEMO safeguard the neurovascular unit. J. Exp. Med. *212*, 1529–1549.

31. Dubrac, A., Künzel, S.E., Künzel, S.H., Li, J., Chandran, R.R., Martin, K., Greif, D.M., Adams, R.H., and Eichmann, A. (2018). NCK-dependent pericyte migration promotes pathological neovascularization in ischemic retinopathy. Nat. Commun. *9*, 3463.

32. András, I.E., Deli, M.A., Veszelka, S., Hayashi, K., Hennig, B., and Toborek, M. (2007). The NMDA and AMPA/KA receptors are involved in glutamate-induced alterations of occludin expression and phosphorylation in brain endothelial cells. J. Cereb. Blood Flow Metab. *27*, 1431–1443.

33. Krizbai, I.A., Deli, M.A., Pestenácz, A., Siklós, L., Szabó, C.A., András, I., and Joó, F. (1998). Expression of glutamate receptors on cultured cerebral endothelial cells. J. Neurosci. Res. *54*, 814–819.

34. Scott, G.S., Bowman, S.R., Smith, T., Flower, R.J., and Bolton, C. (2007). Glutamate-stimulated peroxynitrite production in a brain-derived endothelial cell line is dependent on *N*-methyl-D-aspartate (NMDA) receptor activation. Biochem. Pharmacol. *73*, 228–236.

35. Sharp, C.D., Houghton, J., Elrod, J.W., Warren, A., Jackson, T.H., 4th, Jawahar, A., Nanda, A., Minagar, A., and Alexander, J.S. (2005). *N*-methyl-D-aspartate receptor activation in human cerebral endothelium promotes intracellular oxidant stress. Am. J. Physiol. Heart Circ. Physiol. *288*, H1893–H1899.

36. Zhu, H.J., and Liu, G.Q. (2004). Glutamate up-regulates P-glycoprotein expression in rat brain microvessel endothelial cells by an NMDA receptor-mediated mechanism. Life Sci. *75*, 1313–1322.

37. Ridder, D.A., Lang, M.F., Salinin, S., Röderer, J.P., Struss, M., Maser-Gluth, C., and Schwaninger, M. (2011). TAK1 in brain endothelial cells mediates fever and lethargy. J. Exp. Med. *208*, 2615–2623.

38. Zhang, S.J., Buchthal, B., Lau, D., Hayer, S., Dick, O., Schwaninger, M., Veltkamp, R., Zou, M., Weiss, U., and Bading, H. (2011). A signaling cascade of nuclear calcium-CREB-ATF3 activated by synaptic NMDA receptors defines a gene repression module that protects against extrasynaptic NMDA receptor-induced neuronal cell death and ischemic brain damage. J. Neurosci. *31*, 4978–4990.

39. Abbott, N.J., Rönnbäck, L., and Hansson, E. (2006). Astrocyte-endothelial interactions at the blood-brain barrier. Nat. Rev. Neurosci. *7*, 41–53.

40. Dzamba, D., Honsa, P., and Anderova, M. (2013). NMDA receptors in glial cells: pending questions. Curr. Neuropharmacol. *11*, 250–262.

41. Carmeliet, P., and Ruiz de Almodovar, C. (2013). VEGF ligands and receptors: implications in neurodevelopment and neurodegeneration. Cell. Mol. Life Sci. *70*, 1763–1778.

42. Lohela, M., Bry, M., Tammela, T., and Alitalo, K. (2009). VEGFs and receptors involved in angiogenesis versus lymphangiogenesis. Curr. Opin. Cell Biol. *21*, 154–165.

43. Mauceri, D., Freitag, H.E., Oliveira, A.M., Bengtson, C.P., and Bading, H. (2011). Nuclear calcium-VEGFD signaling controls maintenance of dendrite arborization necessary for memory formation. Neuron *71*, 117–130.

44. Witmer, A.N., Vrensen, G.F., Van Noorden, C.J., and Schlingemann, R.O. (2003). Vascular endothelial growth factors and angiogenesis in eye disease. Prog. Retin. Eye Res. *22*, 1–29.

45. Choi, J.S., Shin, Y.J., Lee, J.Y., Yun, H., Cha, J.H., Choi, J.Y., Chun, M.H., and Lee, M.Y. (2010). Expression of vascular endothelial growth factor receptor-3 mRNA in the rat developing forebrain and retina. J. Comp. Neurol. *518*, 1064–1081.

46. Uhlén, M., Fagerberg, L., Hallström, B.M., Lindskog, C., Oksvold, P., Mardinoglu, A., Sivertsson, Å., Kampf, C., Sjöstedt, E., Asplund, A., et al. (2015). Proteomics. Tissue-based map of the human proteome. Science *347*, 1260419.

47. Saunders, A., Macosko, E.Z., Wysoker, A., Goldman, M., Krienen, F.M., de Rivera, H., Bien, E., Baum, M., Bortolin, L., Wang, S., et al. (2018). Molecular diversity and specializations among the cells of the adult mouse brain. Cell *174*, 1015–1030.e16.

48. Zeisel, A., Hochgerner, H., Lonnerberg, P., Johnsson, A., Memic, F., van der Zwan, J., Häring, M., Braun, E., Borm, L.E., La Manno, G., et al. (2018). Molecular architecture of the mouse nervous system. Cell *174*, 999–1014.e22.

49. Mauceri, D., Hagenston, A.M., Schramm, K., Weiss, U., and Bading, H. (2015). Nuclear calcium buffering capacity shapes neuronal architecture. J. Biol. Chem. *290*, 23039–23049.

50. Hemstedt, T.J., Bengtson, C.P., Ramírez, O., Oliveira, A.M.M., and Bading, H. (2017). Reciprocal Interaction of Dendrite Geometry and Nuclear Calcium-VEGFD Signaling Gates Memory Consolidation and Extinction. J. Neurosci. *37*, 6946–6955.

51. Litke, C., Bading, H., and Mauceri, D. (2018). Histone deacetylase 4 shapes neuronal morphology via a mechanism involving regulation of expression of vascular endothelial growth factor D. J. Biol. Chem. *293*, 8196–8207.

52. Hori, T., Fukutome, M., and Koike, C. (2019). Adeno associated virus (AAV) as a tool for clinical and experimental delivery of target genes into the mammalian retina. Biol. Pharm. Bull. *42*, 343–347.

53. Qu, Y., Liu, Y., Noor, A.F., Tran, J., and Li, R. (2019). Characteristics and advantages of adeno-associated virus vector-mediated gene therapy for neurodegenerative diseases. Neural Regen. Res. *14*, 931–938.

54. Porciatti, V. (2015). Electrophysiological assessment of retinal ganglion cell function. Exp. Eye Res. *141*, 164–170.

55. Baldwin, M.E., Catimel, B., Nice, E.C., Roufail, S., Hall, N.E., Stenvers, K.L., Karkkainen, M.J., Alitalo, K., Stacker, S.A., and Achen, M.G. (2001). The specificity of receptor binding by vascular endothelial growth factor-D is different in mouse and man. J. Biol. Chem. *276*, 19166–19171.

56. Baden, T., Berens, P., Franke, K., Román Rosón, M., Bethge, M., and Euler, T. (2016). The functional diversity of retinal ganglion cells in the mouse. Nature *529*, 345–350.

57. Masland, R.H. (2012). The neuronal organization of the retina. Neuron *76*, 266–280.

58. Sweeney, N.T., James, K.N., Nistorica, A., Lorig-Roach, R.M., and Feldheim, D.A. (2019). Expression of transcription factors divides retinal ganglion cells into distinct classes. J. Comp. Neurol. *527*, 225–235.

59. Guo, S., and Lo, E.H. (2009). Dysfunctional cell-cell signaling in the neurovascular unit as a paradigm for central nervous system disease. Stroke *40* (3, Suppl), S4–S7.

60. Jindal, V. (2015). Neurodegeneration as a primary change and role of neuroprotection in diabetic retinopathy. Mol. Neurobiol. *51*, 878–884.

61. Lok, J., Wang, X.S., Xing, C.H., Maki, T.K., Wu, L.M., Guo, S.Z., Noviski, N., Arai, K., Whalen, M.J., Lo, E.H., and Wang, X.Y. (2015). Targeting the neurovascular unit in brain trauma. CNS Neurosci. Ther. *21*, 304–308.

62. Posada-Duque, R.A., Barreto, G.E., and Cardona-Gomez, G.P. (2014). Protection after stroke: cellular effectors of neurovascular unit integrity. Front. Cell. Neurosci. *8*, 231.

63. Zlokovic, B.V. (2011). Neurovascular pathways to neurodegeneration in Alzheimer's disease and other disorders. Nat. Rev. Neurosci. *12*, 723–738.

64. Hammes, H.P., Federoff, H.J., and Brownlee, M. (1995). Nerve growth factor prevents both neuroretinal programmed cell death and capillary pathology in experimental diabetes. Mol. Med. *1*, 527–534.

65. Hogan-Cann, A.D., and Anderson, C.M. (2016). Physiological roles of non-neuronal NMDA receptors. Trends Pharmacol. Sci. *37*, 750–767.

66. Krueger, M., Bechmann, I., Immig, K., Reichenbach, A., Härtig, W., and Michalski, D. (2015). Blood-brain barrier breakdown involves four distinct stages of vascular

damage in various models of experimental focal cerebral ischemia. J. Cereb. Blood Flow Metab. *35*, 292–303.

67. Ivanova, E., Alam, N.M., Prusky, G.T., and Sagdullaev, B.T. (2019). Blood-retina barrier failure and vision loss in neuron-specific degeneration. JCI Insight *5*, 126747.
68. Nippert, A.R., Biesecker, K.R., and Newman, E.A. (2018). Mechanisms mediating functional hyperemia in the brain. Neuroscientist *24*, 73–83.
69. Feit-Leichman, R.A., Kinouchi, R., Takeda, M., Fan, Z., Mohr, S., Kern, T.S., and Chen, D.F. (2005). Vascular damage in a mouse model of diabetic retinopathy: relation to neuronal and glial changes. Invest. Ophthalmol. Vis. Sci. *46*, 4281–4287.
70. Challa, V.R., Thore, C.R., Moody, D.M., Anstrom, J.A., and Brown, W.R. (2004). Increase of white matter string vessels in Alzheimer's disease. J. Alzheimers Dis. *6*, 379–383, discussion 443–449.
71. Kornzweig, A.L., Eliasoph, I., and Feldstein, M. (1968). Selective atrophy of the radial peripapillary capillaries in chronic glaucoma. Arch. Ophthalmol. *80*, 696–702.
72. Yang, P., Pavlovic, D., Waldvogel, H., Dragunow, M., Synek, B., Turner, C., Faull, R., and Guan, J. (2015). String vessel formation is increased in the brain of Parkinson disease. J. Parkinsons Dis. *5*, 821–836.
73. Lu, L., Hogan-Cann, A.D., Globa, A.K., Lu, P., Nagy, J.I., Bamji, S.X., and Anderson, C.M. (2019). Astrocytes drive cortical vasodilatory signaling by activating endothelial NMDA receptors. J. Cereb. Blood Flow Metab. *39*, 481–496.
74. Christensen, I., Lu, B., Yang, N., Huang, K., Wang, P., and Tian, N. (2019). The susceptibility of retinal ganglion cells to glutamatergic excitotoxicity is type-specific. Front. Neurosci. *13*, 219.
75. Weber, A.J., Kaufman, P.L., and Hubbard, W.C. (1998). Morphology of single ganglion cells in the glaucomatous primate retina. Invest. Ophthalmol. Vis. Sci. *39*, 2304–2320.
76. Shou, T., Liu, J., Wang, W., Zhou, Y., and Zhao, K. (2003). Differential dendritic shrinkage of α and β retinal ganglion cells in cats with chronic glaucoma. Invest. Ophthalmol. Vis. Sci. *44*, 3005–3010.
77. Leung, C.K.S., Lindsey, J.D., Crowston, J.G., Lijia, C., Chiang, S., and Weinreb, R.N. (2008). Longitudinal profile of retinal ganglion cell damage after optic nerve crush with blue-light confocal scanning laser ophthalmoscopy. Invest. Ophthalmol. Vis. Sci. *49*, 4898–4902.
78. Weber, A.J., Harman, C.D., and Viswanathan, S. (2008). Effects of optic nerve injury, glaucoma, and neuroprotection on the survival, structure, and function of ganglion cells in the mammalian retina. J. Physiol. *586*, 4393–4400.
79. Feng, L., Zhao, Y., Yoshida, M., Chen, H., Yang, J.F., Kim, T.S., Cang, J., Troy, J.B., and Liu, X. (2013). Sustained ocular hypertension induces dendritic degeneration of mouse retinal ganglion cells that depends on cell type and location. Invest. Ophthalmol. Vis. Sci. *54*, 1106–1117.
80. Lykken, E.A., Shyng, C., Edwards, R.J., Rozenberg, A., and Gray, S.J. (2018). Recent progress and considerations for AAV gene therapies targeting the central nervous system. J. Neurodev. Disord. *10*, 16.
81. Rodrigues, G.A., Shalaev, E., Karami, T.K., Cunningham, J., Slater, N.K.H., and Rivers, H.M. (2018). Pharmaceutical development of AAV-based gene therapy products for the eye. Pharm. Res. *36*, 29.
82. Margalit, E., and Sadda, S.R. (2003). Retinal and optic nerve diseases. Artif. Organs *27*, 963–974.
83. Majumder, M., Tutunea-Fatan, E., Xin, X., Rodriguez-Torres, M., Torres-Garcia, J., Wiebe, R., Timoshenko, A.V., Bhattacharjee, R.N., Chambers, A.F., and Lala, P.K. (2012). Co-expression of α9β1 integrin and VEGF-D confers lymphatic metastatic ability to a human breast cancer cell line MDA-MB-468LN. PLoS ONE *7*, e35094.
84. Papiewska-Pajak, I., Boncela, J., Przygodzka, P., and Cierniewski, C.S. (2010). Autocrine effects of VEGF-D on endothelial cells after transduction with AD-VEGF-$D^{\Delta N \Delta C}$. Exp. Cell Res. *316*, 907–914.
85. Issaka, R.B., Oommen, S., Gupta, S.K., Liu, G., Myers, J.L., Ryu, J.H., and Vlahakis, N.E. (2009). Vascular endothelial growth factors C and D induces proliferation of lymphangioleiomyomatosis cells through autocrine crosstalk with endothelium. Am. J. Pathol. *175*, 1410–1420.
86. Akahane, M., Akahane, T., Shah, A., Okajima, E., and Thorgeirsson, U.P. (2005). A potential role for vascular endothelial growth factor-D as an autocrine growth factor for human breast carcinoma cells. Anticancer Res. *25* (2A), 701–707.
87. Ahlgren, H., Bas-Orth, C., Freitag, H.E., Hellwig, A., Ottersen, O.P., and Bading, H. (2014). The nuclear calcium signaling target, activating transcription factor 3 (ATF3), protects against dendrotoxicity and facilitates the recovery of synaptic transmission after an excitotoxic insult. J. Biol. Chem. *289*, 9970–9982.
88. Depp, C., Bas-Orth, C., Schroeder, L., Hellwig, A., and Bading, H. (2018). Synaptic activity protects neurons against calcium-mediated oxidation and contraction of mitochondria during excitotoxicity. Antioxid. Redox Signal. *29*, 1109–1124.
89. Oliveira, A.M., Litke, C., Paldy, E., Hagenston, A.M., Lu, J., Kuner, R., Bading, H., and Mauceri, D. (2019). Epigenetic control of hypersensitivity in chronic inflammatory pain by the de novo DNA methyltransferase Dnmt3a2. Mol. Pain *15*, 1744806919827469.
90. Zhang, S.J., Steijaert, M.N., Lau, D., Schütz, G., Delucinge-Vivier, C., Descombes, P., and Bading, H. (2007). Decoding NMDA receptor signaling: identification of genomic programs specifying neuronal survival and death. Neuron *53*, 549–562.